NASA Technical Memorandum 4696

Dynamic and Transient Performance of Turbofan/Turboshaft Convertible Engine With Variable Inlet Guide Vanes

Jack G. McArdle, Richard L. Barth, Leon M. Wenzel,
and Thomas J. Biesiadny

APRIL 1996

National Aeronautics and
Space Administration

NASA Technical Memorandum 4696

Dynamic and Transient Performance of Turbofan/Turboshaft Convertible Engine With Variable Inlet Guide Vanes

Jack G. McArdle, Richard L. Barth, Leon M. Wenzel,
and Thomas J. Biesiadny
Lewis Research Center
Cleveland, Ohio

National Aeronautics and
Space Administration

Office of Management

Scientific and Technical
Information Program

1996

Dynamic and Transient Performance of Turbofan/Turboshaft Convertible Engine With Variable Inlet Guide Vanes

Jack G. McArdle, Richard L. Barth, Leon M. Wenzel, and Thomas J. Biesiadny
National Aeronautics and Space Administration
Lewis Research Center
Cleveland, Ohio

Summary

A convertible engine called the CEST TF34, using the variable inlet guide vane method of power change, was tested on an outdoor stand at the NASA Lewis Research Center with a waterbrake dynamometer for the shaft load. A new digital electronic system, in conjunction with a modified standard TF34 hydromechanical fuel control, kept engine operation stable and safely within limits. All planned testing was completed successfully. Steady-state performance and acoustic characteristics were reported previously and are referenced. This report presents results of transient and dynamic tests. The transient tests measured engine response to several rapid changes in thrust and torque commands at constant fan (shaft) speed. Limited results from dynamic tests using the pseudo-random binary noise technique are also presented. Performance of the waterbrake dynamometer is discussed in an appendix.

Introduction

A convertible engine can produce turbofan thrust, turboshaft power, or any combined thrust and shaft power continuously while operating up to full speed. Convertible engines could be used to power vertical/short-takeoff-and-landing (V/STOL) airplanes and advanced high-speed rotorcraft. For a jet-powered V/STOL airplane the convertible feature could be used to power a remote lifting device, such as a shaft-driven lift fan, or to cross-couple the fans in a two-engine configuration for safety in case one engine should fail. For a rotorcraft a convertible engine would operate as a turboshaft engine to drive a lifting rotor for takeoff and low-speed horizontal flight and as a turbofan engine to produce thrust for high-speed horizontal flight. Analytical studies of high-speed rotorcraft have shown that using a convertible engine rather than separate engines for lift and cruise would give installation, cost, and performance benefits (refs. 1 and 2).

In a convertible engine the power turbine drives both the fan and an output shaft connected to some other load. Total turbine power is the sum of the power absorbed by all the loads, so that any turbine power in excess of what is needed by the fan is available at the power output shaft for other loads. Maximum turbine power is limited by cycle temperature (fuel flow) and speed. For high thrust the shaft load is reduced or decoupled, as by releasing a clutch. When shaft power is required, the fan is unloaded aerodynamically. Two general methods have been devised to unload the fan (ref. 3). One method is based on variable-pitch fan blades—fan power is reduced as the pitch is made "flatter." This method has been demonstrated in tests of engines such as QCSEE (ref. 4), Q-Fan (ref. 5), and Astafan (tested successfully as a convertible engine in a U.S. Army Research and Technology Laboratories test program). The other method is based on variable inlet guide vanes (VIGV) that can be deflected to change fan airflow and inflow swirl—fan power is reduced as the vanes are closed. This method has been demonstrated in fan research tests (ref. 6) and in tests of a high-bypass-ratio turbofan with no output shaft power (ref. 7).

Starting in 1981 the Convertible Engine Systems Technology (CEST) Program began to study the feasibility of the convertible engine concept. The program objectives included defining requirements for convertible engine systems and evaluating an engine using the VIGV method of power change. The system requirements published at that time are given in references 8 to 11. The experimental work was done at the NASA Lewis Research Center using a TF34–400B (8000-lb-thrust class and high bypass ratio) turbofan specially modified to a VIGV convertible engine called the CEST TF34. The tests were performed on an outdoor test stand with a waterbrake dynamometer for the shaft load. A new digital electronic system was used to control engine speed and variable-geometry actuators. The digital system worked in conjunction with a modified standard TF34 hydromechanical fuel control to keep the CEST engine operation stable and safely within design limits. The test objectives were to demonstrate the performance characteristics of the engine and control system and to obtain data and experience applicable to the design of future convertible propulsion systems.

All planned testing was completed successfully. Results of the steady-state engine performance tests are given in reference 12, and results of fan acoustic tests, in reference 13. This

report describes the results of transient and dynamic tests using the digital engine control system. The transient tests measured engine response to several rapid changes in thrust and torque commands at constant fan speed. During these tests an enigmatic 80-msec dead time, between command start and the beginning of engine geometry or fuel flow change, was discovered. Limited results from dynamic tests using the pseudorandom binary noise (PRBN) technique are also presented. Some of the dynamic data were not evaluated in detail because of the possible effects of the 80-msec dead time.

Typical test results are discussed to bring out important engine and control system characteristics. The remaining data are presented in appropriate graphical format without comment. The engine performed satisfactorily in all the tests.

Performance of the waterbrake dynamometer, a useful shaft load for many applications, is discussed in appendix A. The pseudorandom binary noise generator is described in appendix B. Symbols are defined in appendix C.

Apparatus

Engine

The test engine was a previously used TF34–400B specially modified by the manufacturer in the fan section, as sketched in figure 1. The standard TF34 is a 6:1-bypass-ratio turbofan that can produce 9100 lb of sea-level-static thrust. The single-stage fan is driven by a four-stage, low-pressure turbine. The core has a 14-stage axial compressor, an annular combustor, and a two-stage, high-pressure turbine.

The engine modifications, shown in more detail in figure 2, were made by using as many existing parts as feasible. The resulting configuration, called the CEST TF34, was not meant to be a production engine. The fan was unloaded aerodynamically by deflecting part-span VIGV to change the rate and swirl angle of the flow entering the fan tip. The vanes were "part span" because they reached only from the outer wall to the core/bypass flow splitter and thus had little effect on core flow. When the vanes were deflected, the fan air load was reduced and the power turbine could drive an external load through the power output shaft.

Each major modification is described in the following paragraphs. For more detail consult references 12 and 13.

Variable inlet guide vanes (VIGV).—A set of 30 vanes was installed just ahead of the fan rotor to unload the fan in the turboshaft power mode. Each vane consisted of a fixed forward strut and a movable rear flap. The flaps were deflected together in the direction of fan rotation with hydraulic actuators and a unison ring. The actuators were a General Electric (GE) J101 master/slave system with integral servomechanisms and position sensors. VIGV position normally ranged from 0° (fully open, straight ahead) to +84° (nearly closed). For the dynamic tests the flaps were moved beyond the fully open position (as far as –7°) for VIGV perturbations around 0°.

Variable exit guide vanes (VEGV).—A set of 44 tandem airfoils replaced the same number of standard TF34 exit

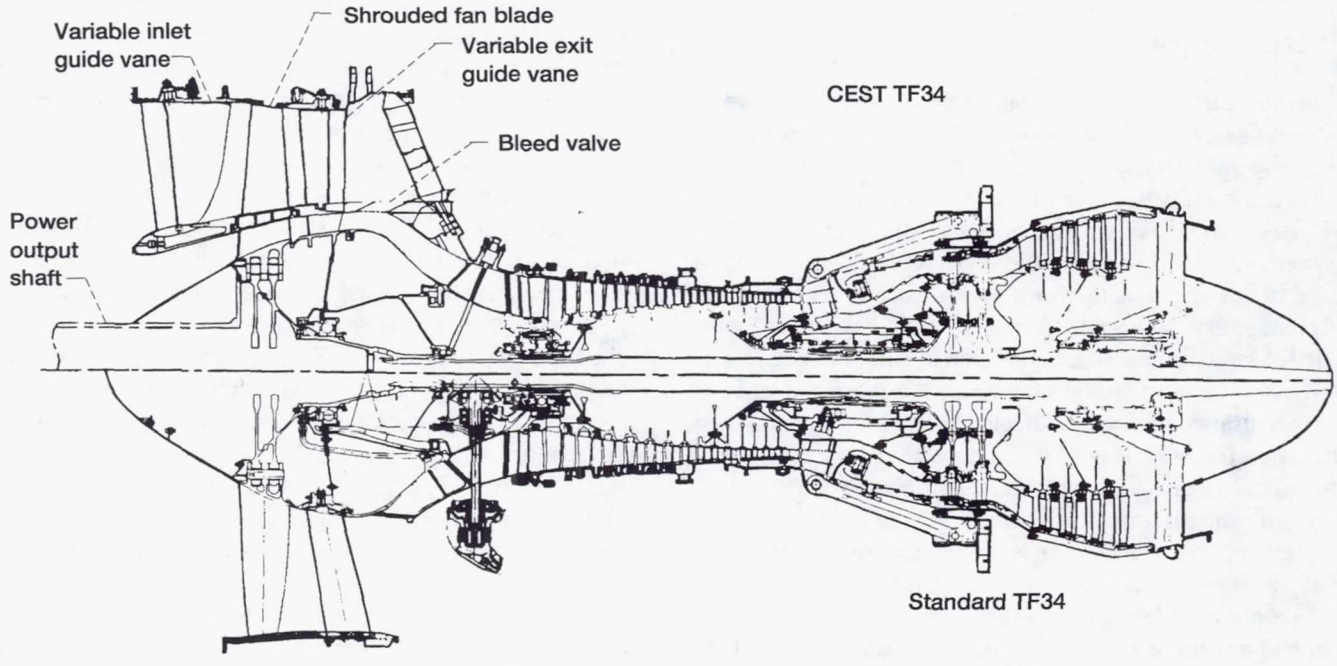

Figure 1.—CEST TF34 convertible engine compared with standard TF34 engine.

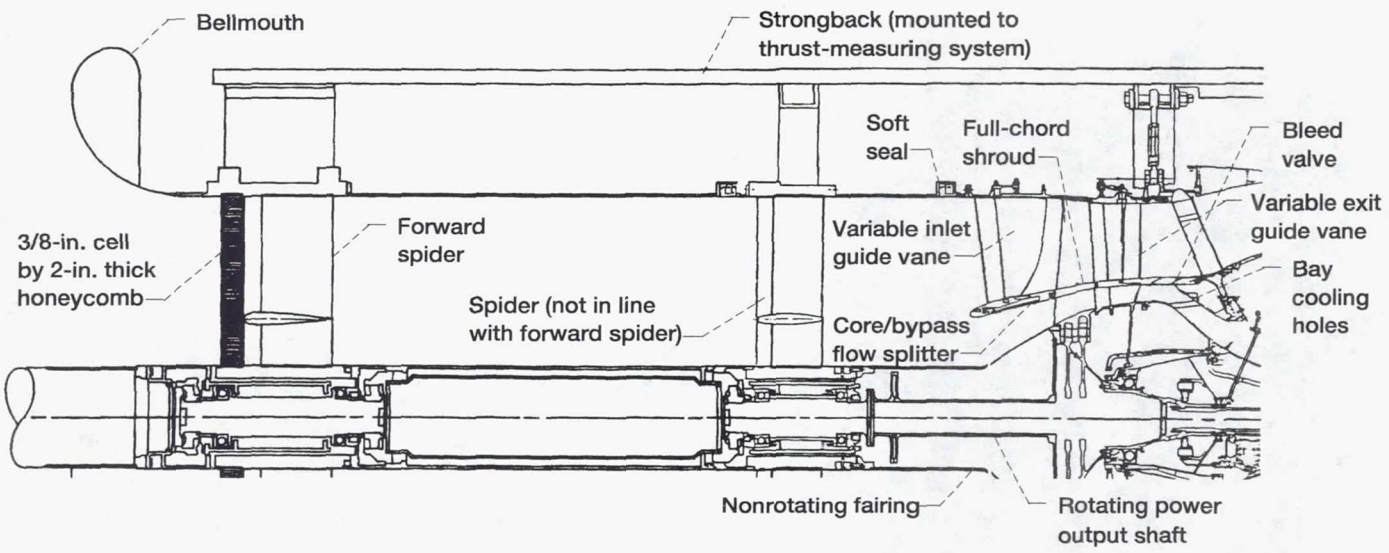

Figure 2.—CEST TF34 design features.

stator vanes in the fan-tip (bypass) flow. The front foils were deflected together with hydraulic actuators and a unison ring. The deflection angle was scheduled to the VIGV deflection to prevent stall buffeting at high VIGV closure. The rear VEGV foils were not movable. The actuators were a GE J101 master/slave system with integral servomechanisms and position sensors.

Power output shaft.—The power output shaft was attached to the fan disk and extended forward through the bellmouth air inlet. The extension included a flexible coupling and bearings supported by spider struts built into the inlet ducting.

Flow splitter.—The core/bypass flow splitter was extended forward to the VIGV to minimize core inlet flow distortion from the deflected VIGV. Shrouds on the fan blades were part of the splitter.

Fan.—The fan rotor had 28 blades. In the tip region the blade airfoils were the same shape as standard TF34 blades but included a part-span shroud (part of the modified flow splitter). In the hub region a revised shape was used to improve core pumping. The fan was the same as that used for the steady-state tests reported in reference 12.

Bleed valve (BV).—A core/bypass bleed valve was installed in the flow splitter behind the VEGV to improve the flow match between the fan hub and the core engine at low-power operation. The valve was a sliding ring valve moved by three GE J101 actuators with modified F404 servomechanisms and position sensors.

Inlet and exhaust.—All testing was done with a bellmouth and long inlet duct having a combination honeycomb flow straightener and protective screen (fig. 2). The engine had the standard TF34 separate-flow, nonadjustable exhaust nozzles.

Test Stand

The CEST TF34 installed on the outdoor static test stand at NASA Lewis is shown in figure 3. The engine was mounted on a strongback and suspended from an overhead thrust system capable of measuring up to 10 000-lb thrust. The engine power output shaft was connected to a waterbrake dynamometer by a driveline supported on a pedestal. The driveline contained several crowned splines to take up misalignment.

Hydraulic power from a facility system having a 23-gal/min pump and a 5-gal accumulator provided actuator power for the engine variable geometry and the waterbrake flow control valve.

Power Absorber System

The power absorber system, shown schematically in figure 4, controlled power output shaft torque and provided the shaft power load. The power-absorbing device was a waterbrake dynamometer operated up to 5300 hp as described in appendix A. The waterbrake was coupled directly to the engine power output shaft. Shaft torque was varied by positioning the 4-in. exit water flow valve, which had a linear plug (CV = 175) actuated at 2800 psig with a 2.5-in. cylinder, 2.5-in. stroke, and 15-gal/min servovalve. Water throughflow was set by the bypass valve. The outflow was collected in an open sump and then pumped back to the cooling tower supply. The waterbrake capability, rated by the manufacturer, is shown in figure 5.

Torque was controlled by a closed-loop system that positioned the exit water valve using feedback from a strain-gage

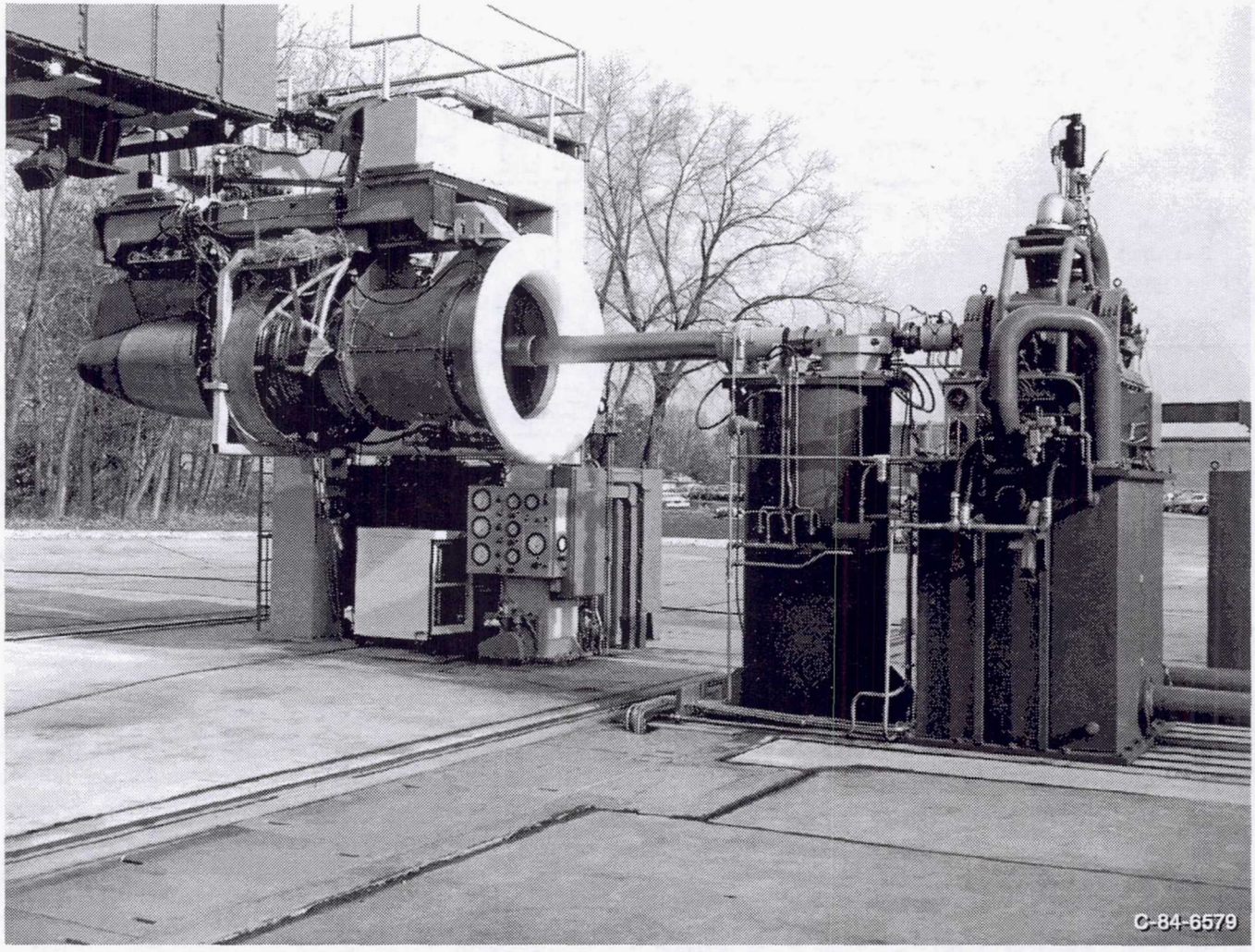

Figure 3.—CEST TF34 engine and waterbrake power absorber installed at outdoor static test stand at NASA Lewis Research Center.

load cell on the waterbrake torque arm. Input could be chosen from a manual potentiometer, a signal generator, or a programmable function generator.

Performance of the power absorber system is discussed in appendix A, which also describes an earlier waterbrake configuration.

Instrumentation and Data System

Transducers and measurement systems conventionally used for engine performance had adequate frequency response, so that special instrumentation was not needed. For these tests the following types of instrumentation were used:

(1) Pressure: scanivalves
(2) Temperature: thermocouples
(3) Fuel flow: beam-type flowmeter
(4) Forces: strain-gage load cells
(5) VIGV, VEGV, and water valve position: potentiometers
(6) BV position: linear variable differential transformers
(7) Speeds: magnetic pickups plus electronic counters

Steady-state data were recorded on the laboratory central digital data system. Transient and dynamic data were recorded on magnetic tape. In many cases the steady-state portions of transducer outputs were "bucked" with an analog computer to improve resolution of the time-varying portion of the data.

Digital Electronic Engine Control

A specially designed digital electronic engine control (DEEC) system worked in conjunction with a modified standard TF34 hydromechanical fuel control to keep the CEST engine operation stable and safely within design limits. Operation was divided into two modes: "thrust" mode, for

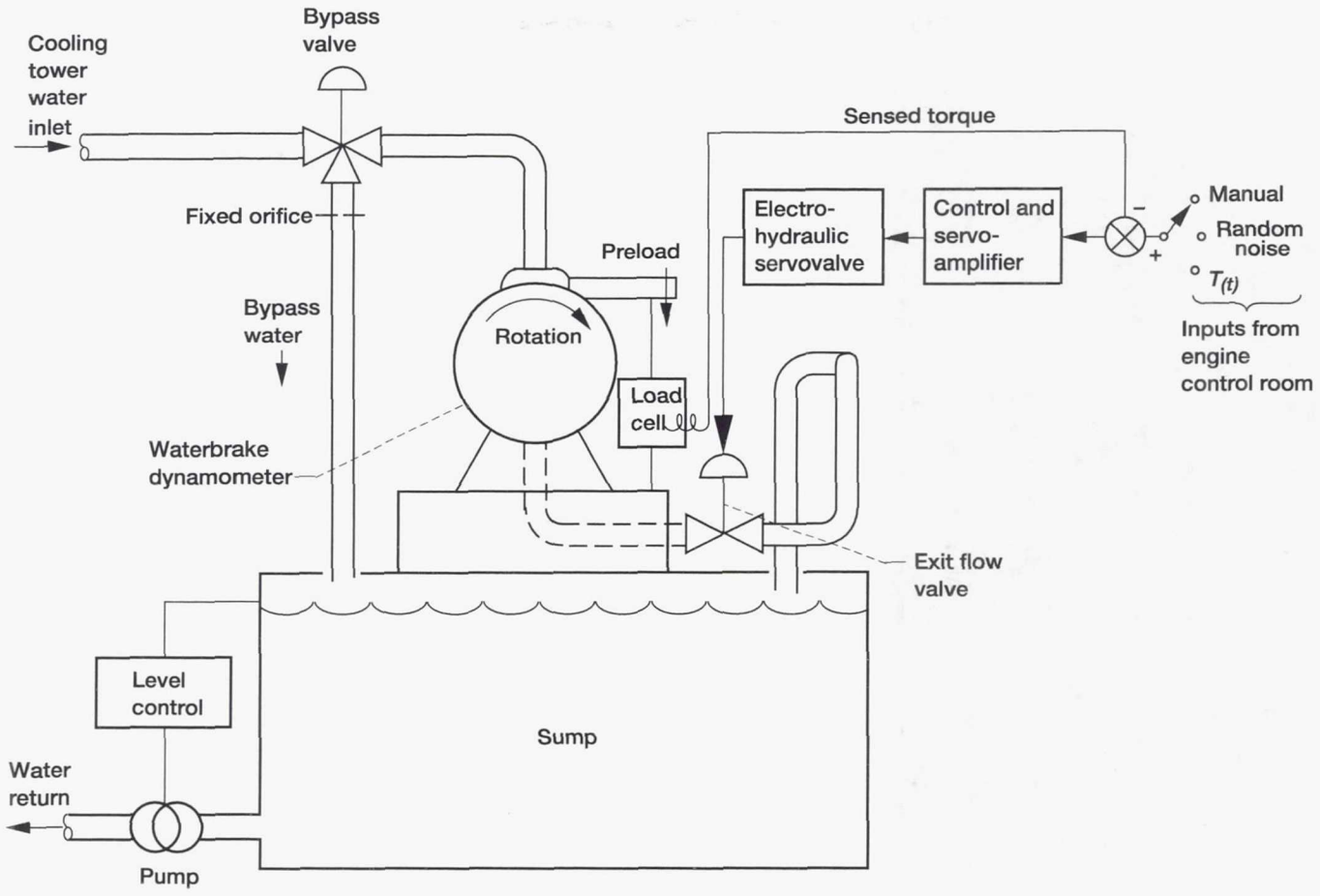

Figure 4.—Power absorber (waterbrake dynamometer with control valve at exit) system.

turbofan-powered flight, and "shaft" mode, for rotary-wing or twin-engine V/STOL flight. In either mode the engine could produce shaft power and thrust up to the limiting power turbine inlet temperature. The control strategy for each mode is illustrated in figure 6. In the shaft mode both the engine thrust level and the shaft speed were commanded. The control system, using feedback data from the engine, set fuel flow and engine variable geometry to maintain shaft (fan) speed as the power output shaft load changed. In the thrust mode only the thrust level was commanded. The system locked the VIGV in the fully open position and adjusted fuel flow to bring the fan to a preprogrammed speed to produce the command thrust. A block diagram of the engine control system is presented in figure 7. (For some tests the inputs and signal paths shown in figure 7 were changed to measure specific data. The changes are described along with the appropriate test results.) Important features of the system are described in the following paragraphs. Design philosophy, control schematic diagram, and predicted operating characteristics are discussed fully in reference 14.

Inputs.—For these tests the inputs consisted of a manual potentiometer setting for the reference shaft speed; a manual potentiometer setting, signal generator, or programmable function generator signal for thrust command; and the standard TF34 power lever (which set a core-speed governor) for reference core speed. After engine start the power lever was advanced to maximum so that performance was not limited by core speed.

Mode switch.—The manually operated mode switch changed control logic by some relatively simple circuit changes in the digital control. This was an important feature of the CEST TF34 engine control system because the two control strategies could be implemented with the same hardware equipment.

Reference shaft speed schedule.—The DEEC set fan speed from a preprogrammed schedule to produce the desired thrust. The actual thrust was not sensed by the control. The schedule was set up for zero shaft power and was not adjusted for variations in thrust caused by changes in core speed, such as brought about by shaft load changes.

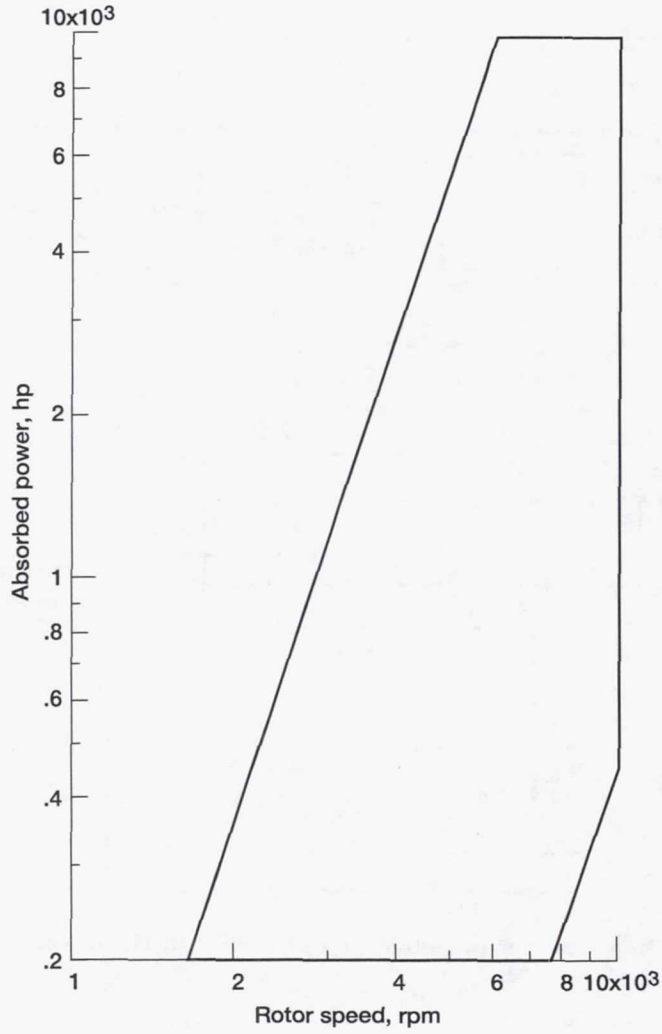

Figure 5.—Rated waterbrake capability.

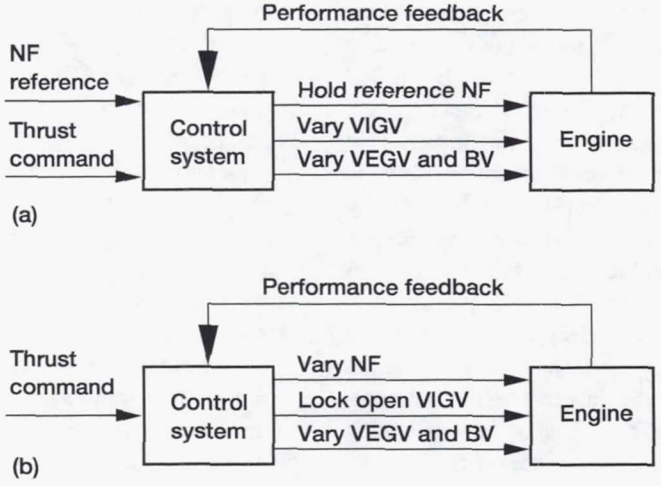

Figure 6.—CEST TF34 control strategies. (a) Shaft mode. (b) Thrust mode.

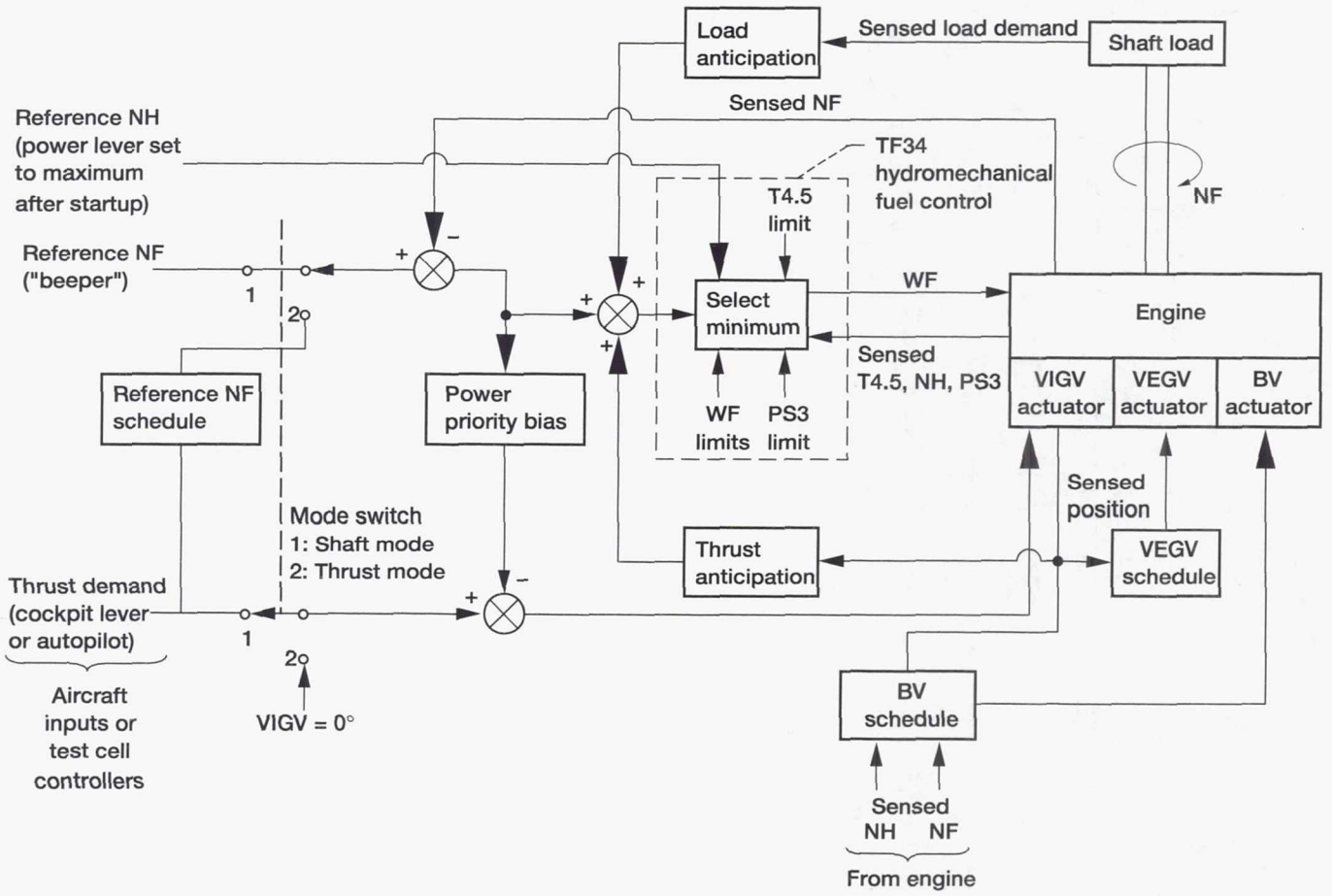

Figure 7.—Block diagram of CEST TF34 engine control system.

Engine variable geometry.—The VIGV, VEGV, and BV were driven by hydraulic actuation systems with proportional-plus-integral position controls. The VIGV closure angle was set by the thrust command signal as modified by the power priority bias. The VEGV angle was set to a preprogrammed schedule based on experimental data (ref. 12). The BV opening was varied to a complex schedule by using VIGV, core speed, and shaft speed data. This schedule was determined analytically and was not investigated further during the testing.

TF34 hydromechanical fuel control.—A standard TF34 fuel control was modified for the CEST TF34. The modifications consisted of expanding the authority of a trim torquemotor, which manipulated the fuel-metering valve. The new authority limits extended from slightly above "idle" power to maximum power. In this range the torquemotor accepted electrical signals from the digital control and positioned the metering valve in response. Also, the null bias on the torquemotor was changed to provide fail-safe action (decreasing fuel flow) if current were lost.

The limits built into the control to ensure safe engine operation were not changed.

Anticipation.—Anticipation circuits caused a transient variation in fuel flow for sudden changes in torque or thrust demand in order to minimize speed droop or overshoot. The fuel transients were proportional to the rate at which demand changed, but a deadband centered around zero rate prevented anticipation for gradual demand adjustments. The thrust anticipation was taken from the VIGV position signal. For the tests the load anticipation was taken from the waterbrake torque command; in an aircraft, anticipation could come from any of several possible loads, such as rotor collective pitch or power change in a lifting fan.

Power priority bias.—With large shaft load, commands for high thrust would cause shaft speed to droop if power-turbine inlet temperature or fuel flow reached a limit before the desired thrust level was attained. This shaft speed droop might be unacceptable for rotorcraft applications because of rotor lift loss. The power priority bias circuits overcame this droop by reducing the VIGV command when shaft speed fell 2 percent or more below the reference speed.

Layout and support equipment.—The layout of the control system and its support equipment is shown in figure 8. The control and its power supply were located in the test cell in a

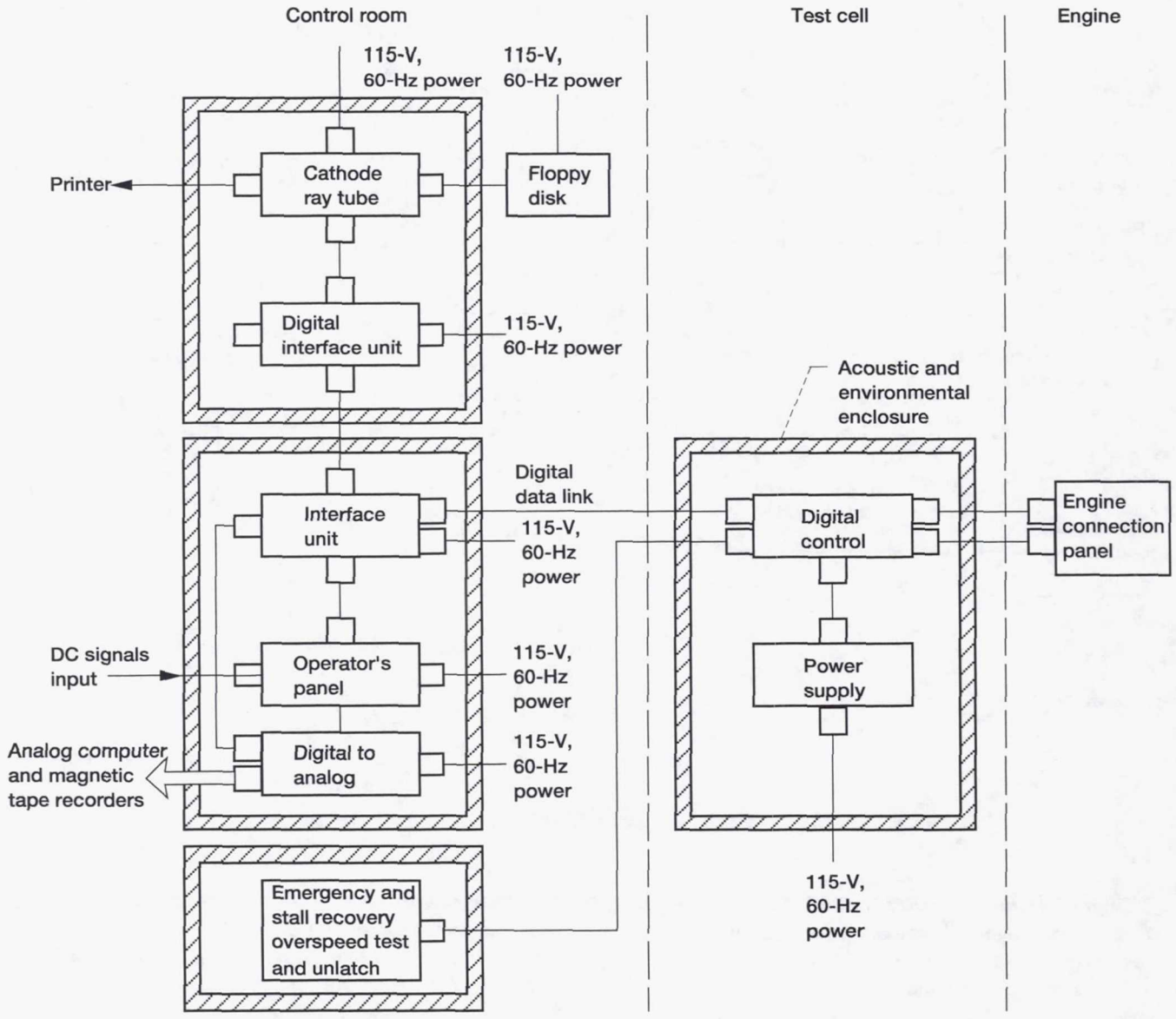

Figure 8.—Layout of CEST TF34 engine control system.

cabinet near the engine. The control contained the computer, the control algorithm on programmable read-only memories (PROM's), and all electronics needed for the digital functions. The control was connected to the engine and to equipment in the control room with shielded electrical cables.

In the control room the operator's panel contained 50 potentiometers and 16 switches that could be used to modify schedules, gains, and limits in the digital control. This panel received the thrust and reference speed commands and the torque command signal for the power anticipation circuit. A digital-to-analog converter unit provided up to 25 buffered control system outputs for recording or display. Recording was done on magnetic tape and strip charts. Many of the data channels were routed through an analog computer to amplify the time-varying portion of the data for better resolution. The video display was used to monitor system setup and operation with a program that resided on a floppy disk. The video display could be printed at the operator's request. The emergency shutdown and overspeed test panel contained switches to accomplish those functions.

Procedure

Transient Tests

Just before making a transient test the engine was set to each end point by using the DEEC operator's controls, and the performance was recorded for calibration. The engine was reset to the starting point by using the DEEC in the selected

mode, and the test was performed by applying signals from a programmable function generator to the thrust and torque command inputs. The data were recorded on magnetic tape.

Dynamic Tests

For open-loop frequency response tests the engine was set at the desired steady-state operating condition by using the DEEC and then perturbed a small amount on either side of this condition. The steady-state data were recorded for calibration. To perform the test, the PRBN generator signal (see appendix B) was applied to the appropriate input, and dynamic data were recorded on magnetic tape for 8 min. For the constant-fuel-flow tests the fan speed feedback signal to the hydromechanical fuel control was disconnected and replaced with an equivalent signal from a facility signal generator. This technique was used so that the fan speed could vary in response to its changing load and without control reaction while keeping the limits and engine safety features provided by the control.

Data Processing

Digital.—The steady-state performance data were averaged over several scans of the sampling pattern. Performance parameters were computed from the averaged data on a mainframe computer.

Transient.—The recorded data were played back on strip charts calibrated from the end-point digital data.

Dynamic.—Control-room strip chart data were used for initial test evaluation. The taped dynamic data were digitized off-line at 50 samples per second for plotting or for analysis with existing computer programs. Frequency response data were processed in the frequency domain with a fast Fourier transfer (FFT) program. The transfer functions were calculated with the data-fit program described in reference 15. In this program the anticipated form of the transfer function was input and then constants were manipulated to obtain the best simultaneous fit (least mathematical residue) between the FFT results and the program's computed amplitude ratio and phase angle.

Results and Discussion

Operating Principles

The CEST TF34 is a high-bypass-ratio turbofan engine. At sea-level-static operation most of the thrust is produced by the fan discharging through an unchoked, convergent exhaust nozzle of fixed area. As indicated on the generic fan map sketched below, closing the VIGV has the effect of moving constant-speed lines toward lower flow and pressure rise. The load line is unchanged because the exhaust nozzle size is fixed.

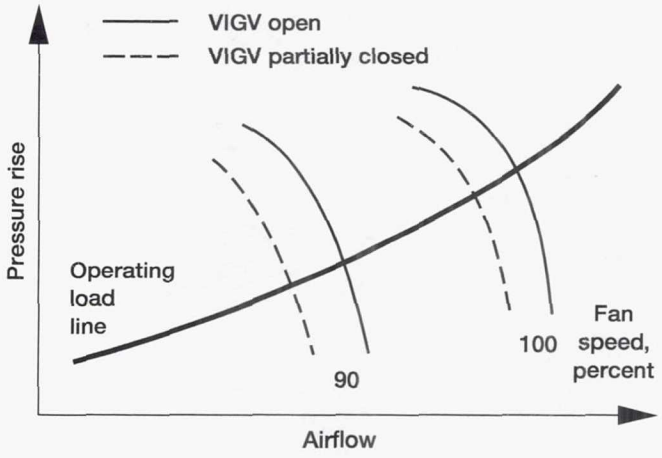

This characteristic is used to unload the fan. On a VIGV type of convertible engine turbine power is then available to drive an output shaft load. On a V/STOL aircraft the VIGV could be used to modulate fan thrust for hover flight.

To provide a background for the discussion of the dynamic test results, the sea-level-static operational characteristics of the CEST TF34 engine (taken from ref. 12) are illustrated in figure 9. At each constant fan (shaft) speed (fig. 9(a)) operation is bounded by performance with the VIGV open (high-thrust region), with the VIGV closed (low-thrust, high-shaft-power region), and with limiting power-turbine inlet temperature, $T4.5_{max}$. Lines showing performance at constant VIGV angle and constant T4.5 are called out in the figure. In the high-thrust region closing the VIGV unloads the fan, and turbine power becomes available at the shaft. In the low-thrust region closing the VIGV continues to reduce fan flow, but the fan compression efficiency decreases significantly and shaft power levels off. The fan absorbs power by churning and heating the relatively stagnant air in the fan duct, although a small amount of air flows through for cooling. Zero thrust is not attained mainly because of residual core thrust. At each speed maximum shaft power is produced with the VIGV closed at $T4.5_{max}$.

The operating envelope (fig. 9(b)) consists of many planes of constant-fan-speed performance maps. With no shaft power and the VIGV open, the engine behaves like a conventional turbofan and produces maximum thrust at $T4.5_{max}$ and 100-percent fan speed, NF_{max}. Within the total operating envelope any combination of thrust and shaft power can be obtained by appropriately positioning the VIGV and adjusting T4.5 (fuel flow). Transient and frequency response tests were made at several points within the operating envelope. The engine ran smoothly and stably for all the tests.

Transient Test Results

Transient tests were performed to explore engine behavior throughout the operating envelope at 95-percent referred fan speed NF_R. The nominal transient test paths are shown in

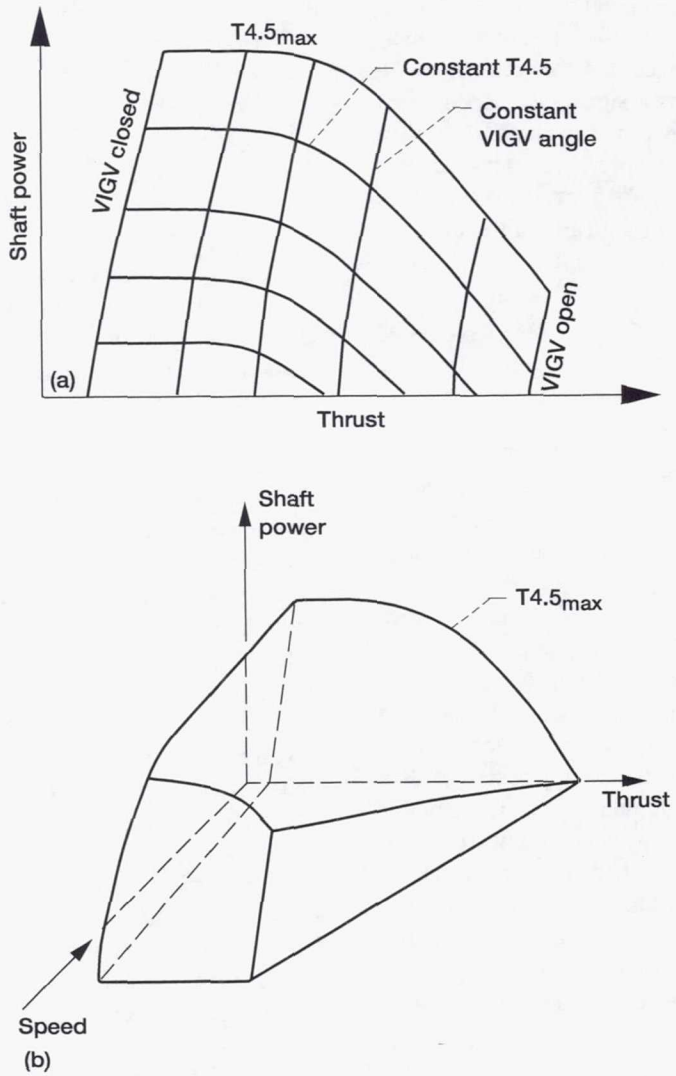

Figure 9.—Operational characteristics of CEST TF34 engine. (a) Performance at constant fan (shaft) speed. (b) Operating envelope.

figure 10. Unless otherwise noted, the tests were performed in the "shaft" control mode with all the control loops active except the power priority bias, and the anticipation circuits were set at nominal gain. The thrust command and reference fan speed were input to the DEEC (see fig. 6), and the torque command was applied to the waterbrake control (see fig. 4). The waterbrake provided the shaft load and had fast, but sometimes nonlinear, response to the torque command as discussed in appendix A. No additional rotary inertia or damping was added to the power output shaft. The waterbrake inertia was small relative to the combined inertia of the fan and the power turbine, so that the results closely approximate the behavior of the engine alone.

The strip charts from each test show both increasing and decreasing transients. An 80- to 120-msec delay (or dead time) occurred between the command signal and the beginning of engine geometry or fuel flow changes, as illustrated in figure 11. The consistent occurrence of this dead time suggests that it is inherent in the engine control or facility apparatus, but the cause is not explainable by the engine manufacturer or in the use of the facility control or data acquisition equipment.

Large torque steps.—The engine responded effectively to large torque changes commanded in 0.1 sec at low and high thrust levels, as shown in figures 12 and 13, respectively. The steps were performed at fixed VIGV position. For increasing torque the transient behavior was the same for both cases. Torque rose smoothly toward the new end value after an initial delay but overshot by 500 ft-lb. The new steady-state value was attained within 2 sec. Thrust also increased because of greater core thrust, although no thrust change was commanded. Anticipation circuits gave an initial fuel surge, causing overtorque in the power turbine and increases in rotor speeds. Then the speed control reacted to reduce fuel flow, causing rotor speeds to fall back. Fan speed drooped as much as 400 rpm (6 percent) from the reference speed. The overshoot could be reduced by optimizing the anticipation circuitry gain, and the droop could be minimized by optimizing the fuel/speed loop gain.

When torque decreased, the engine behavior was similar, except that torque and rotor speeds did not overshoot their end values as much as when torque increased.

Large thrust steps.—Large thrust changes were made in both thrust mode (fig. 14) and shaft mode (fig. 15). In thrust mode the VIGV was locked fully open and thrust was varied by fan speed. In this mode the CEST engine performed as a conventional turbofan engine and changed thrust level stably to the new end value. The anticipation loop in the DEEC was inactive because the VIGV did not move (see fig. 7), and engine operation was safely limited by the hydromechanical fuel control. Thrust changes were completed in about 2 sec for both increasing and decreasing steps, and the waterbrake control system held torque reasonably steady.

In shaft mode the reference fan speed was held constant and thrust was varied by VIGV deflection. The engine responded to commands much more quickly in this mode because the fan did not have to accelerate. Thrust changes were essentially completed within 0.5 sec. The data suggest that

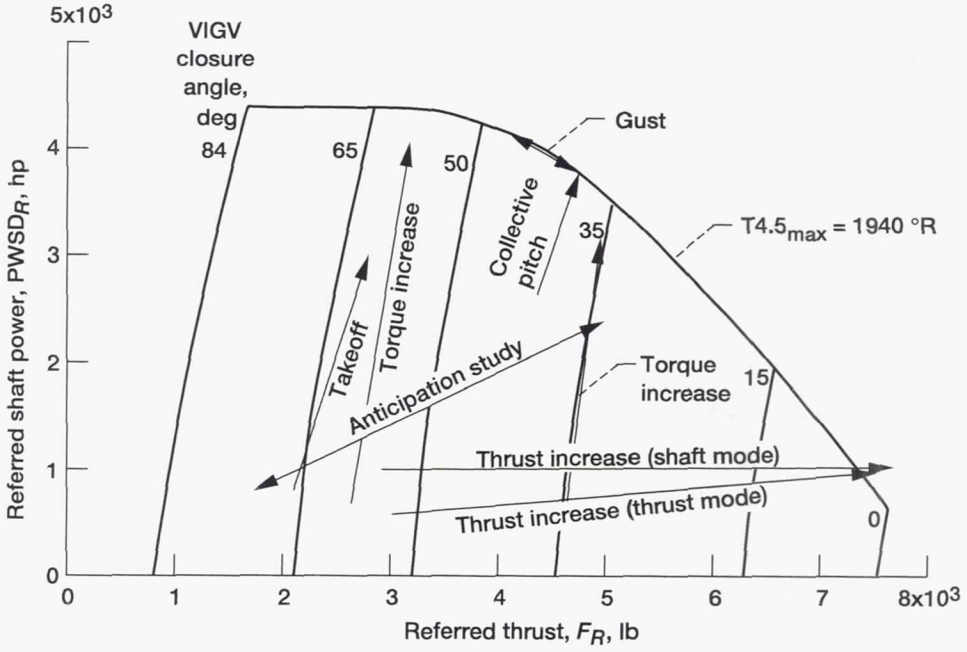

Figure 10.—Nominal transient test paths.

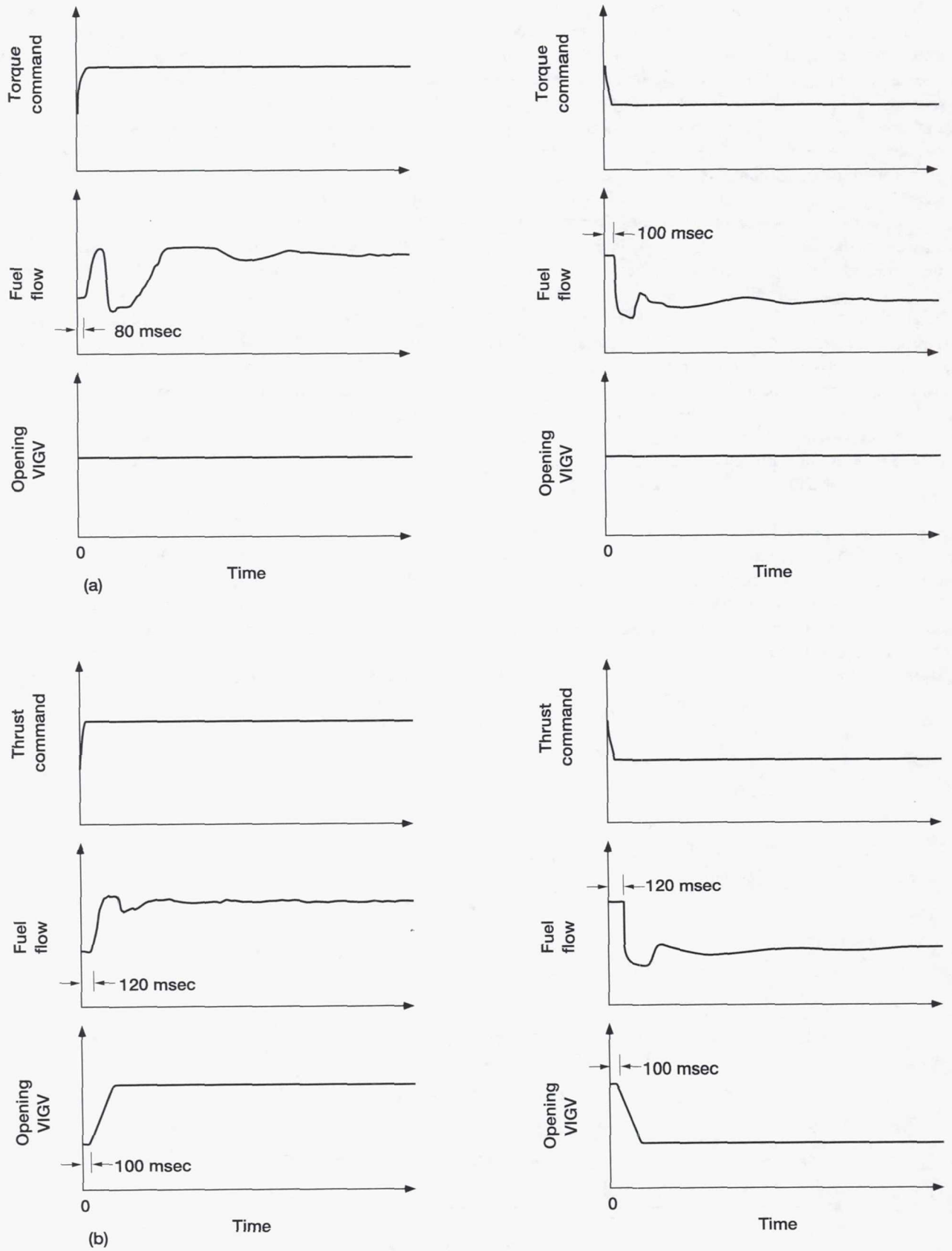

Figure 11.—Typical response delays from start of torque or thrust command. (a) Torque command. (b) Thrust command.

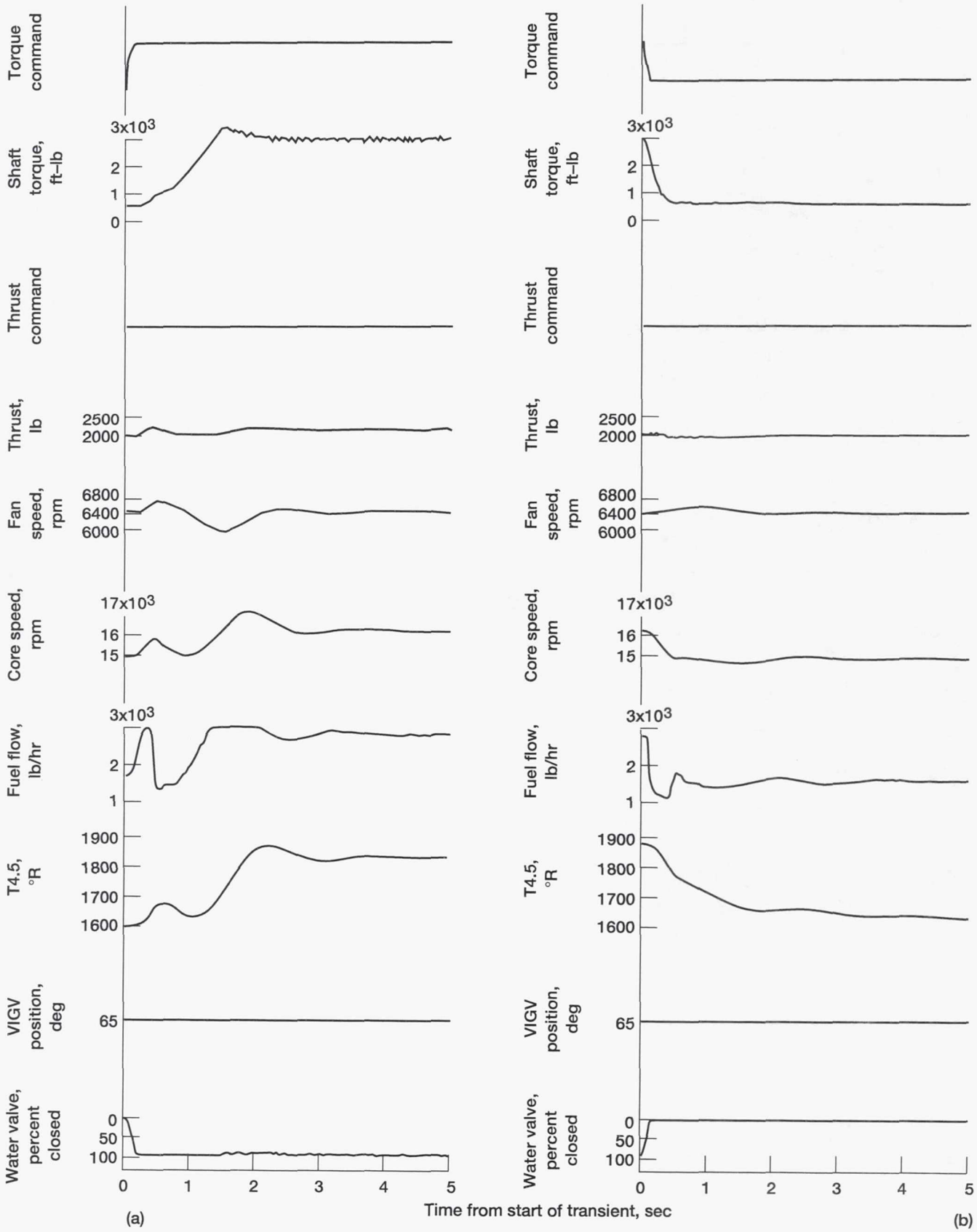

Figure 12.—CEST TF34 performance during large torque steps at low thrust level. (a) Increasing torque. (b) Decreasing torque.

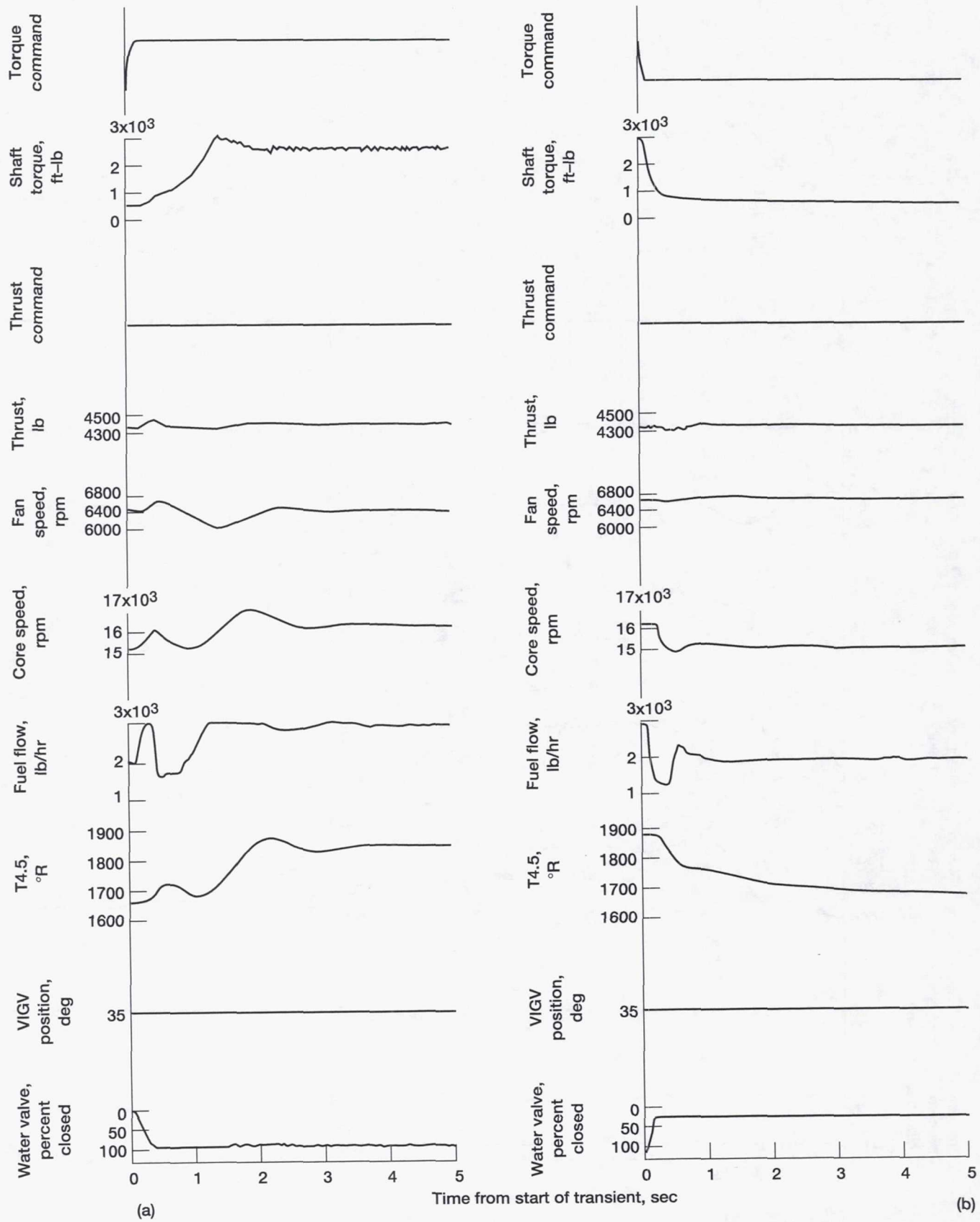

Figure 13.—CEST TF34 performance during large torque steps at high thrust level. (a) Increasing torque. (b) Decreasing torque.

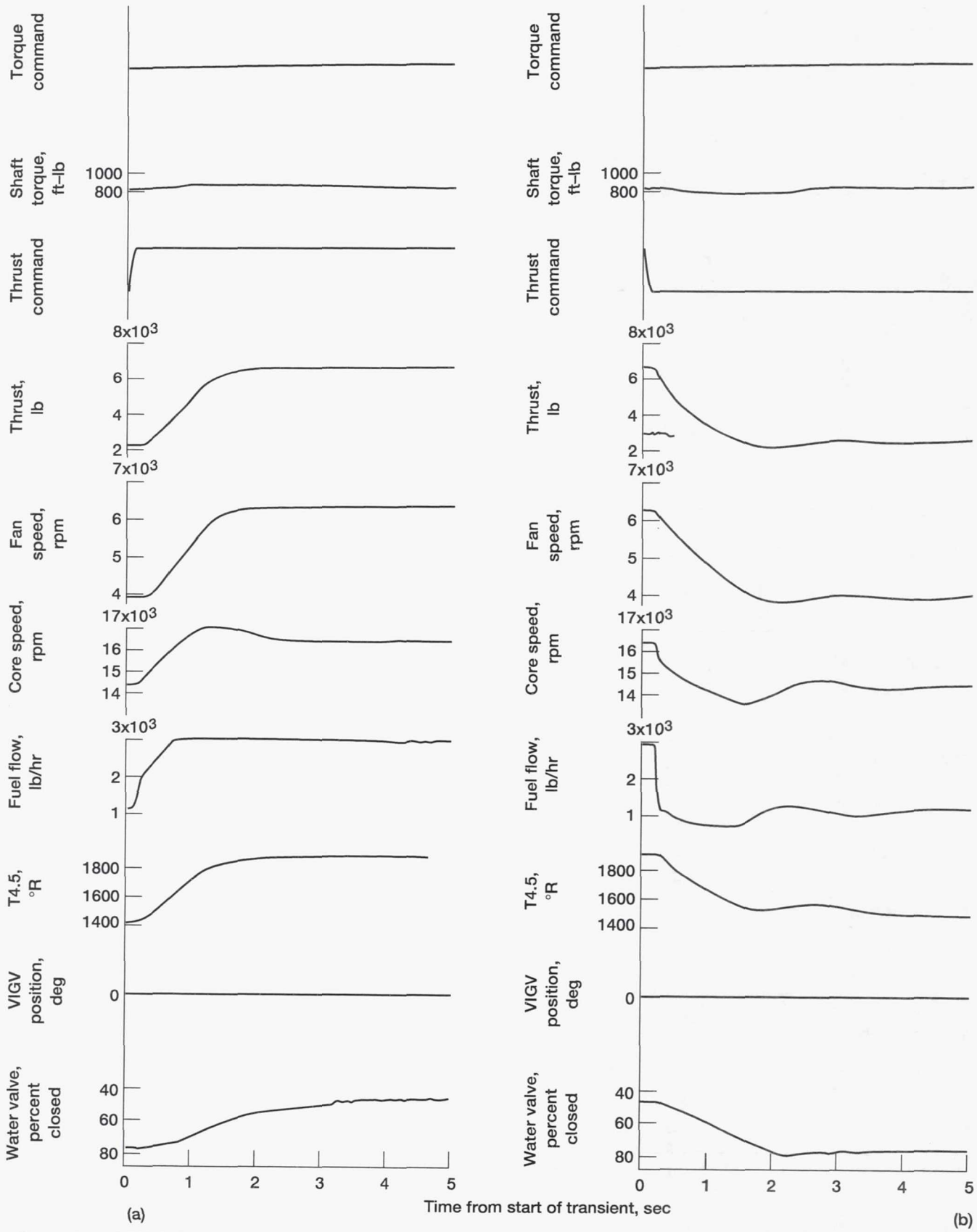

Figure 14.—CEST TF34 performance during large thrust steps in thrust mode. (a) Increasing torque. (b) Decreasing torque.

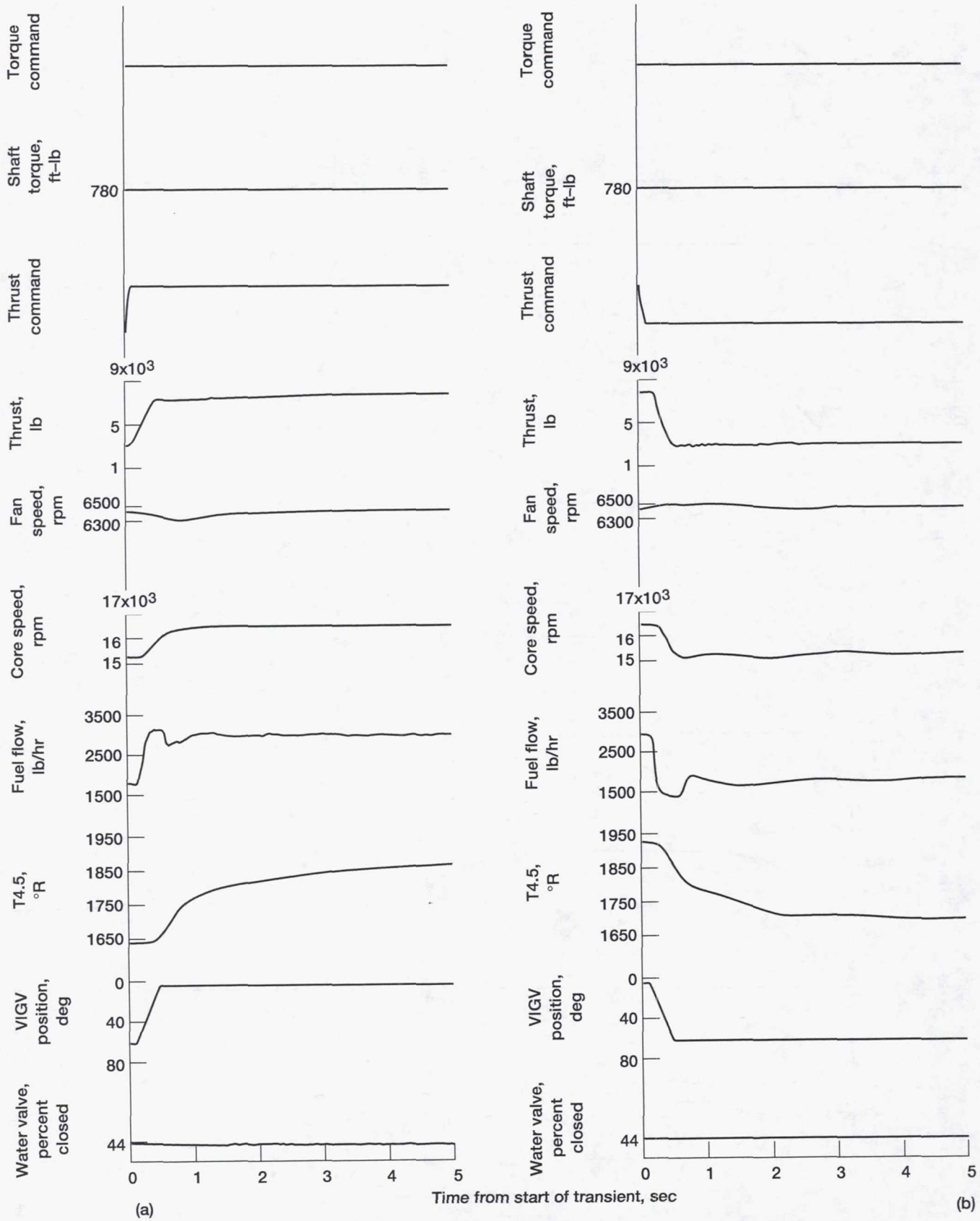

Figure 15.—CEST TF34 performance during large thrust steps in shaft mode. (a) Increasing torque. (b) Decreasing torque.

the response time was limited by the VIGV slewing rate. The measured fan speed overshoot and droop (fig. 15) were about 200 rpm (3 percent of reference fan speed), and the thrust ramps were smooth. The anticipation circuits worked effectively during fuel flow changes. Torque remained steady because the speed changes were small.

Combined transients.—A transient consisting of both thrust and torque changes is shown in figure 16. For this case the anticipation circuits were disabled. The increasing transient began with the waterbrake exit valve operating in a region where torque did not change much with valve position (see fig. 28). This initial insensitivity, possibly coupled with valve starting stiction, caused torque to begin to rise slowly. Speed drooped as torque and thrust increased, and fuel flow increased to bring speed back to the reference speed. During the decreasing transient the sudden torque reduction allowed the fan to overspeed.

A slower combined transient with anticipation circuits active is shown in figure 17. Fan speed initially increased owing to the anticipation fuel surge and the absence of torque change. Thrust increased owing to VIGV opening plus higher fan speed. The fan speed control loop changed fuel flow to correct speed as necessary, but speed did not return to the reference value for about 5 sec after the transient began. Behavior was similar for the decreasing transient, except that torque began to fall with no delay.

Rotorcraft transients.—Transients of the types encountered by advanced rotorcraft were suggested by requirements taken from reference 8. Figure 18 shows engine behavior during a collective pitch change with thrust for an antitorque jet and directional control. For the increasing transient, torque ramped smoothly with the torque command. Shaft speed initially increased because of the anticipation fuel surge but dropped when the VIGV opened. Thrust responded to VIGV change. Speed never quite returned to the reference value because T4.5 reached its limit. The reverse transient showed no unusual behavior.

Engine performance during a simulated unexpected gust encounter is shown in figure 19. Before the gust the engine was running near $T4.5_{max}$. The engine and control responded effectively to commands simulating expected load changes by holding shaft speed steady through the gust.

Open-Loop Frequency Response Tests

Open-loop frequency response tests (engine only) were made with the DEEC in the shaft control mode by using the PRBN technique (see appendix B). As noted in the previous section an unexplained 80- to 120-msec dead time was measured in the transient tests. The same dead time may have been present in these tests; however, it is not accounted for in the data analysis or in the following discussion. Another dead time, in waterbrake response (see appendix A), was not considered important to the results because torque was nearly constant during these tests.

VIGV perturbations.—The open-loop response of the engine to small perturbations in VIGV position is shown in figures 20 and 21. For these tests the fan speed feedback signal to the DEEC was replaced with a dummy steady signal in order to eliminate the effects of fuel flow changes on engine variables. Waterbrake torque was held constant with fixed inlet and exit valve positions.

The steady-state response of engine variables to VIGV position changes at the open (0°) position, a high-thrust, low-shaft-power region, is summarized in figure 20(a). As the VIGV was closed, the fan-tip adiabatic compression efficiency remained high, and fan speed increased to absorb the available turbine power. When speed was higher, the fan-hub discharge pressure increased and the bleed valve flow increased; both of these conditions reduced the core-inlet referred flow and the core rotor speed. The net result of all these changes was to keep thrust relatively constant over this range of VIGV closure angles.

Important open-loop transfer functions are given in figures 20(b) to (d). The fan speed transfer function has a single lag due to the rotary inertia of the fan system consisting of fan, power turbine, shafts, and shaft load. The core speed transfer function contains two lag terms numerically similar to the fan system inertia term. The thrust transfer function contains a derivative term and a lag term. The derivative term may be related to pressure in the fan discharge duct, which varied in phase with fan speed at low frequencies but lagged speed changes as frequency increased. However, no pressure measurements were made to study that argument. At still higher frequencies the fan speed response was attenuated and thrust changes leveled off. Thrust changes probably would have returned to zero at frequencies higher than plotted in figure 20(d).

Results of the same type of test, but with the VIGV closed down to 65°, are shown in figure 21. This is a low-thrust, high-shaft-power region where thrust, but not shaft power, was affected by VIGV position (see fig. 9). Over the range of VIGV angles tested (fig. 21(a)) fan-tip efficiency and flow rate both decreased as VIGV closure increased, and turbine power needed to drive the fan at steady speed was nearly constant. Thrust fell off because about half the thrust came from the fan. Rotor speed and core operation were not changed.

The fan speed transfer function (fig. 21(b)) shows that dynamic effects were much smaller than for the open-VIGV case, but detailed interpretation of the data is difficult. Thrust response (fig. 21(c)) remained constant over the range of frequencies tested.

Fuel flow perturbation.—Results of other open-loop tests in which fuel flow rate was the driving function are shown in figures 22 and 23. For these tests the fan-speed feedback signal to the DEEC was replaced with a driver signal from an external source, thereby effecting a fuel flow perturbation.

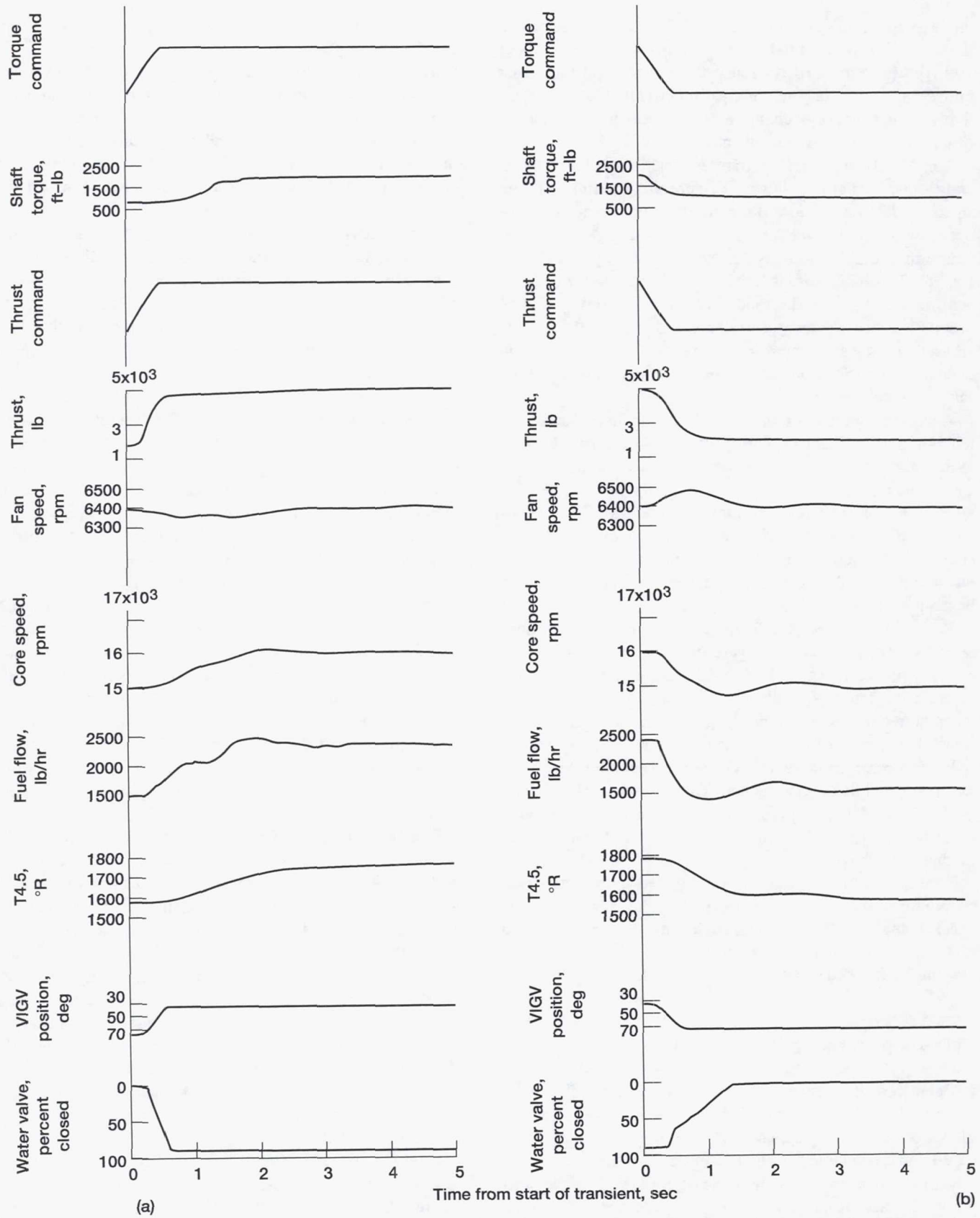

Figure 16.—CEST TF34 performance during combined torque and thrust changes without anticipation circuits. (a) Increasing torque. (b) Decreasing torque.

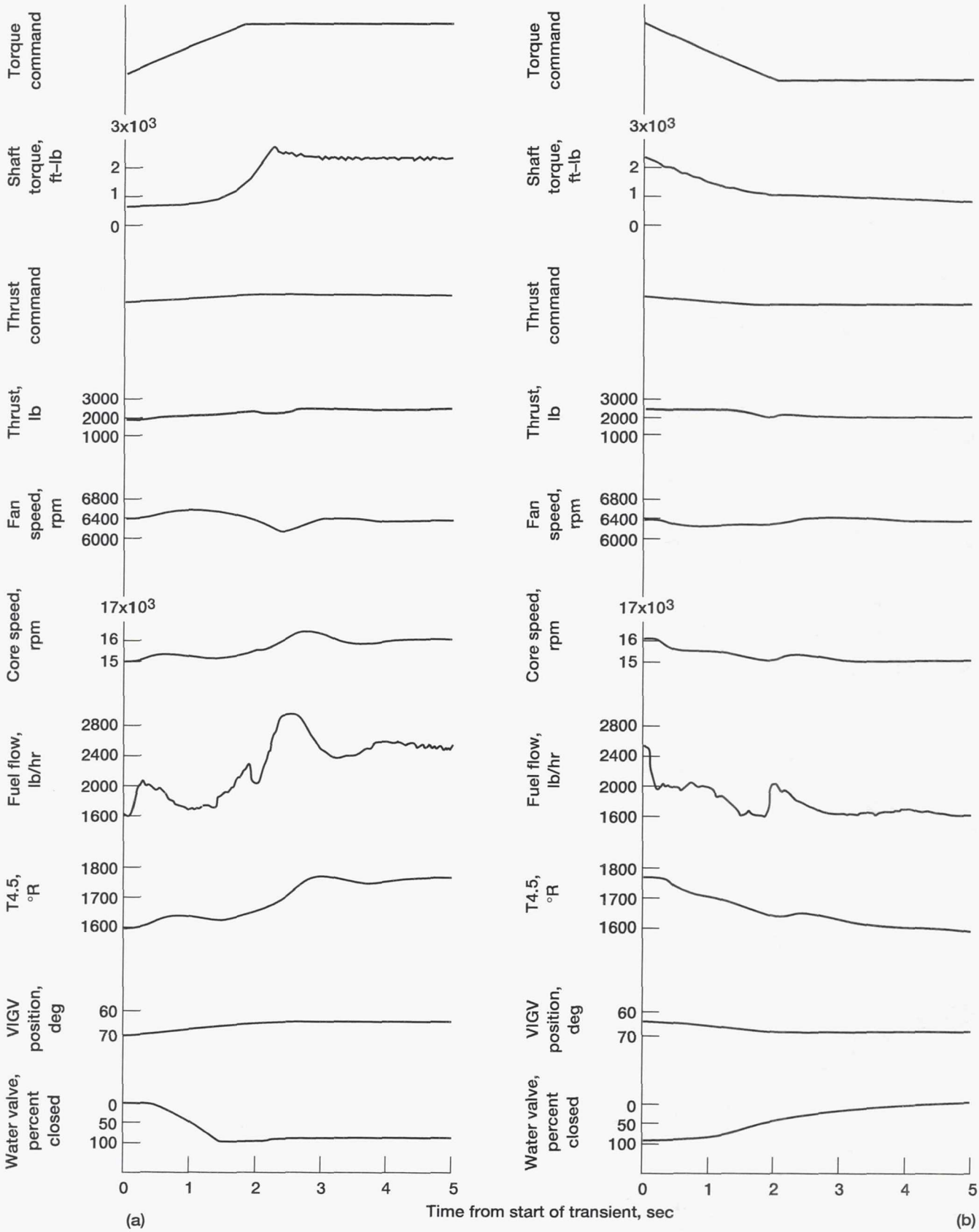

Figure 17.—CEST TF34 performance during combined torque and thrust changes with anticipation circuits. (a) Increasing torque. (b) Decreasing torque.

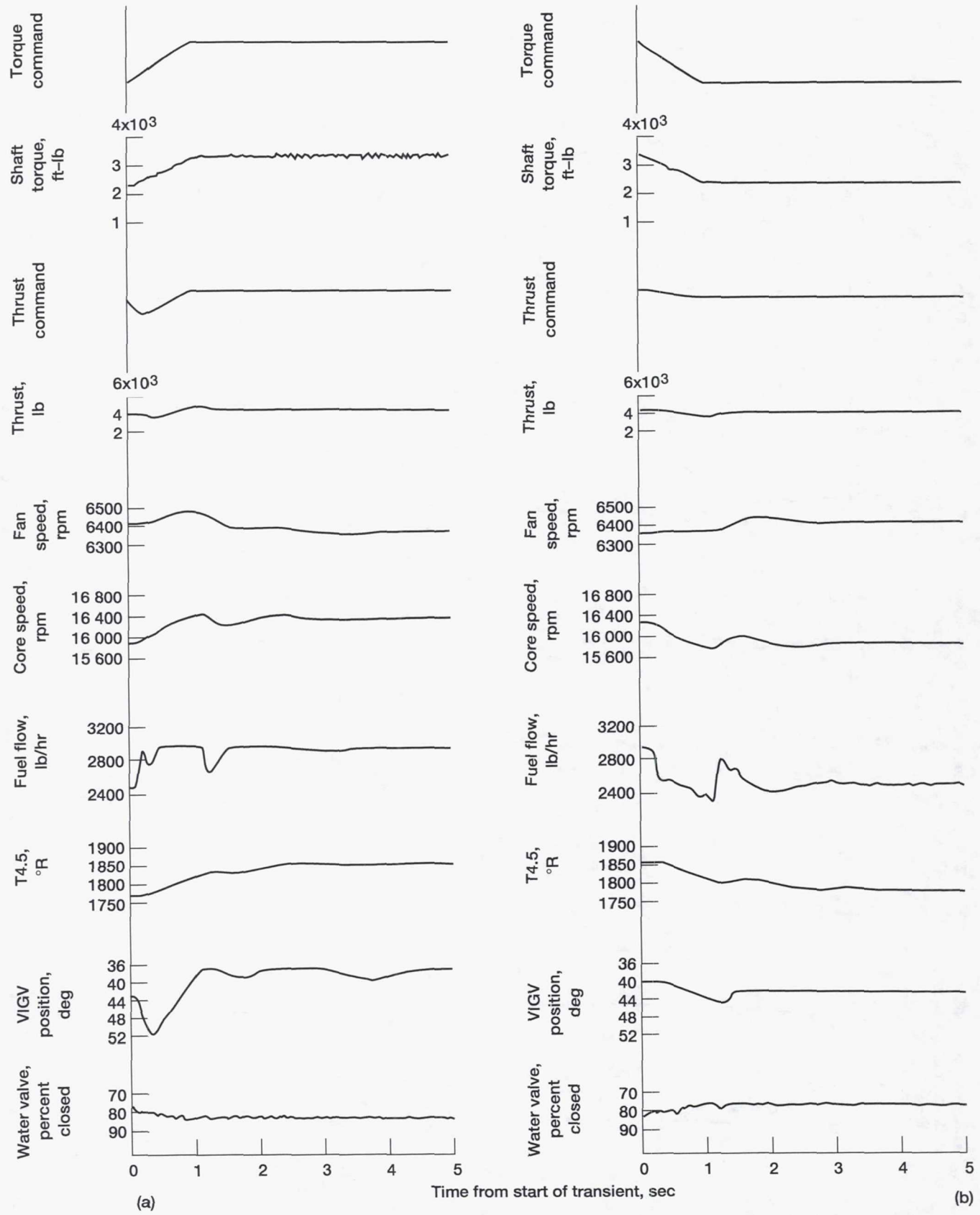

Figure 18.—CEST TF34 performance during simulated collective pitch changes, with power priority bias loop active. (a) Increasing torque. (b) Decreasing torque.

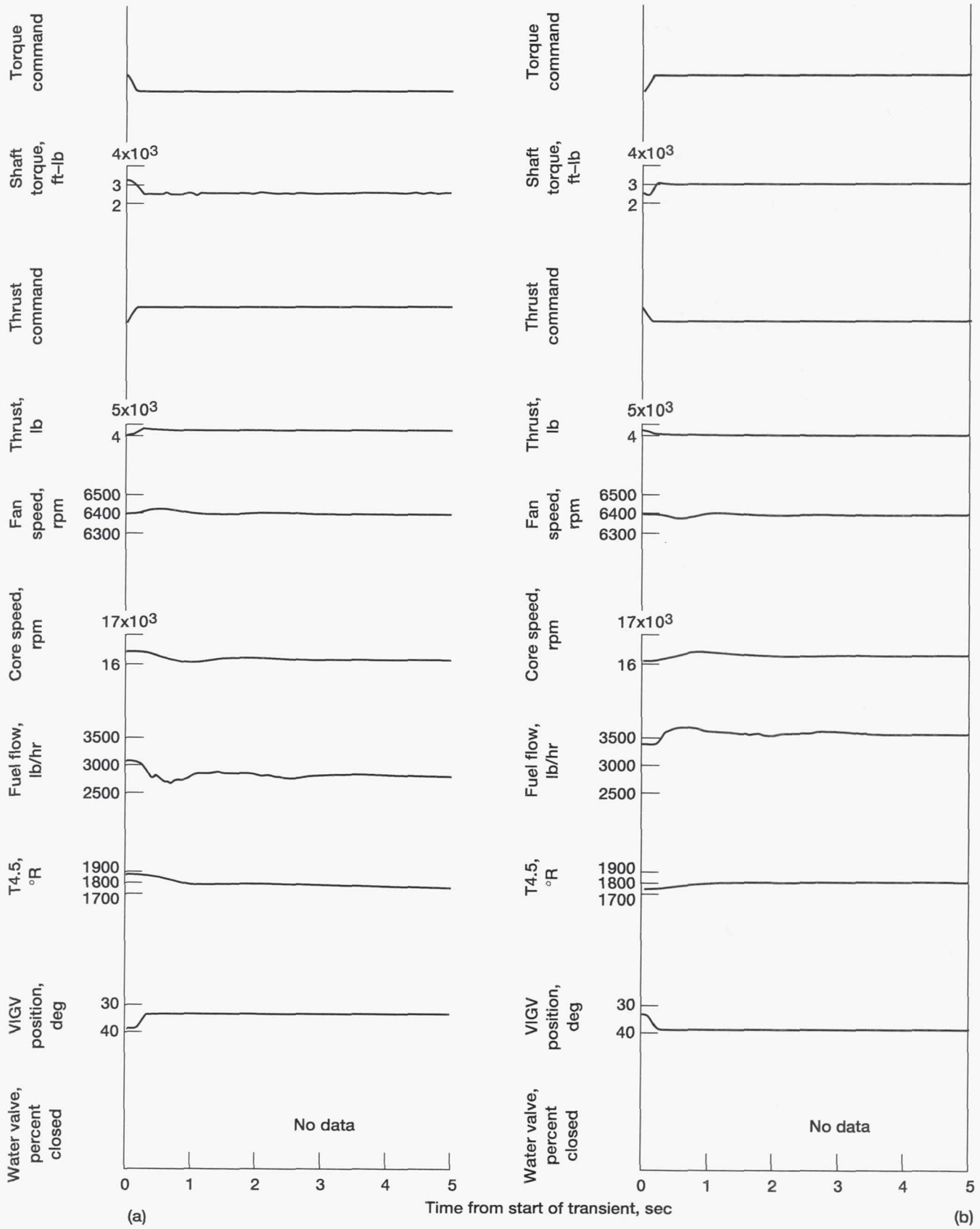

Figure 19.—CEST TF34 performance during simulated unexpected gust encounter (anticipation circuits inactive). (a) Increasing torque. (b) Decreasing torque.

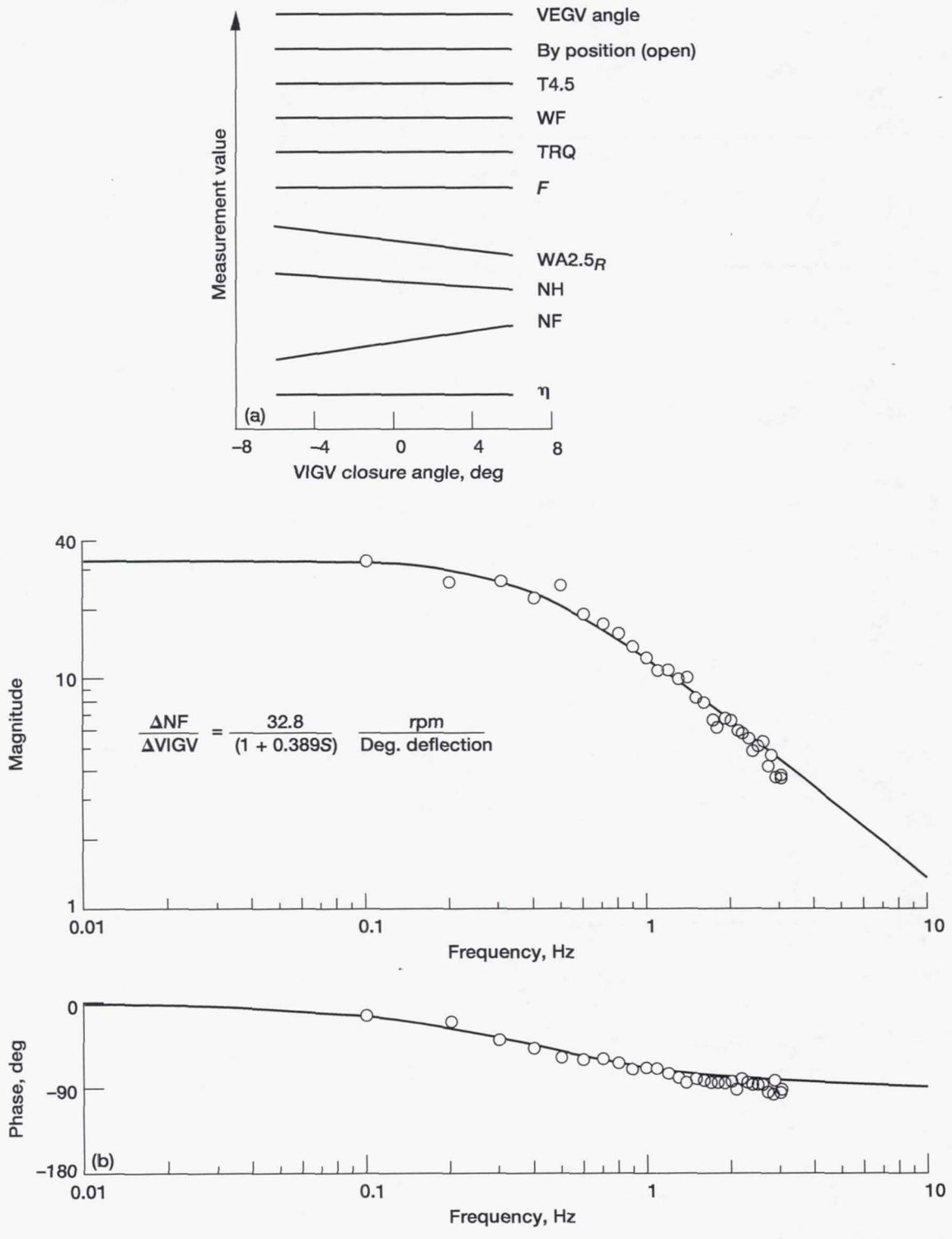

Figure 20.—Open-loop tests with small VIGV perturbations in shaft mode: VIGV open (0°); T4.5 ≃$T4.5_{max}$; NF ≃ 90 percent; PWSD ≈ 640 hp; anticipation circuits and power priority bias off. (a) Steady-state calibration. (b) Fan speed response. (c) Core engine speed response. (d) Thrust response.

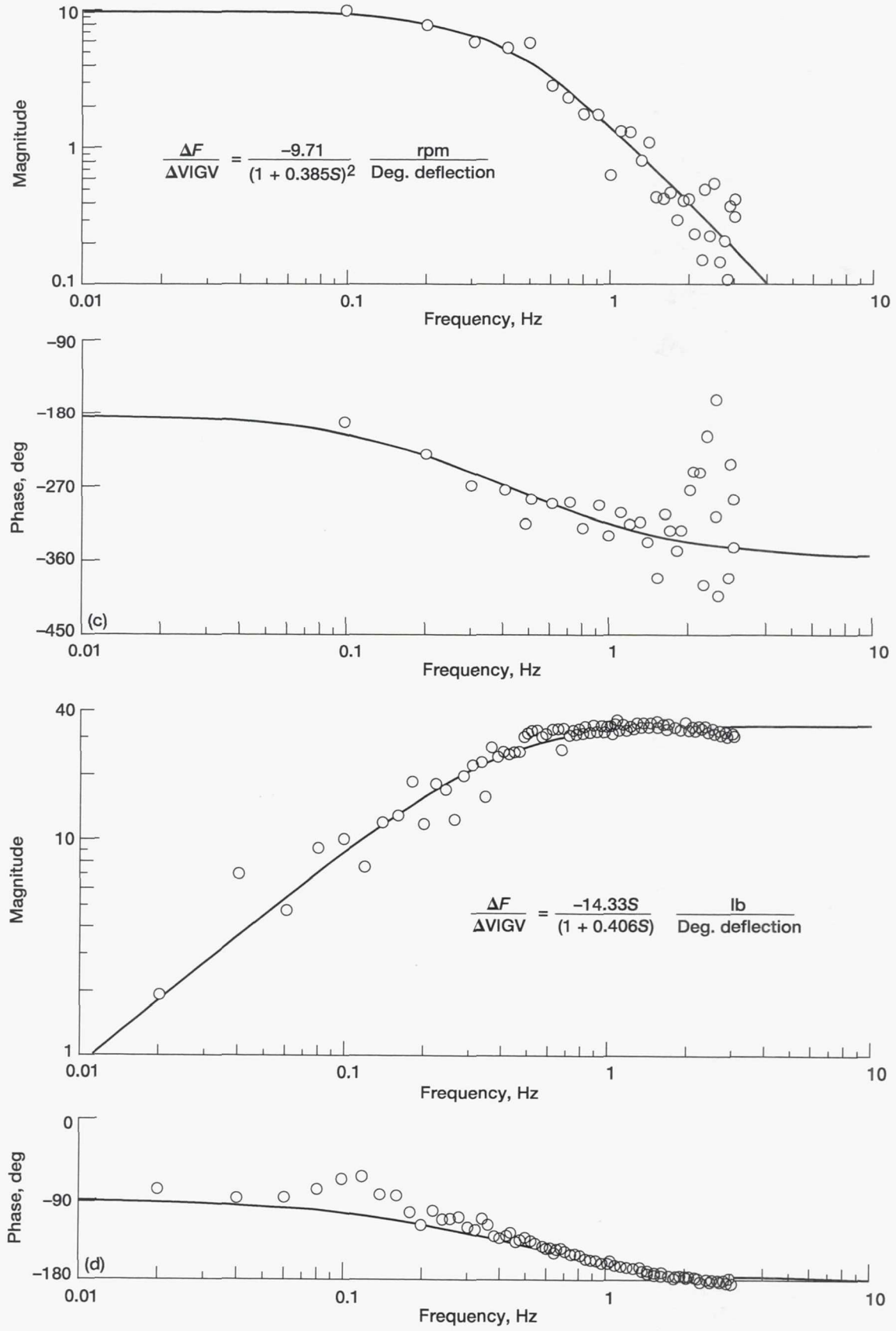

Figure 20.—Concluded. (c) Core engine speed response. (d) Thrust response.

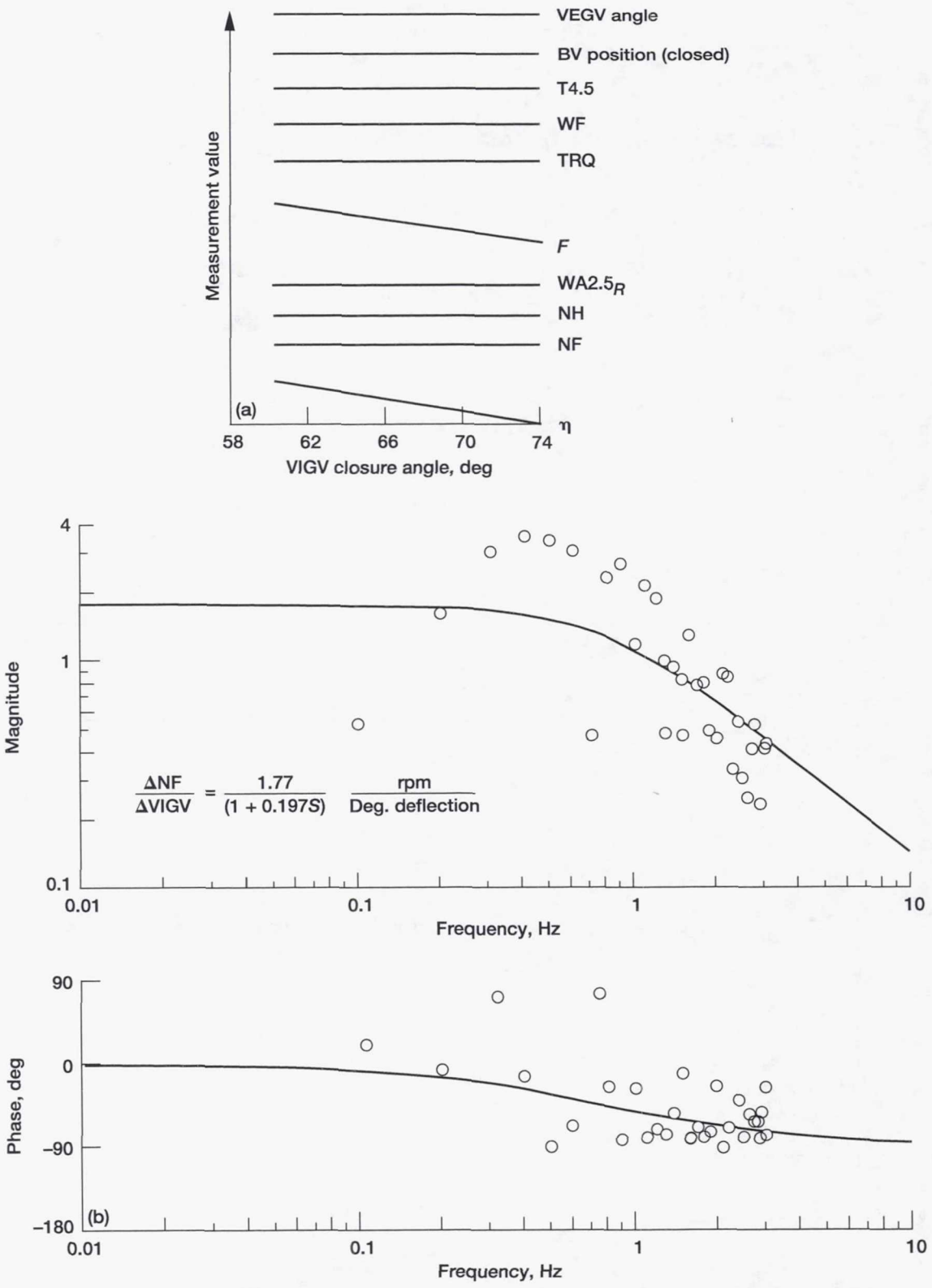

Figure 21.—Open-loop tests with small VIGV perturbations in shaft mode: VIGV closure, 75 percent; T4.5 $\simeq$T4.5$_{max}$; NF $\simeq$ 90 percent; PWSD $\approx$ 3700 hp; anticipation circuits and power priority bias off. (a) Steady-state calibration. (b) Fan speed response. (c) Thrust response.

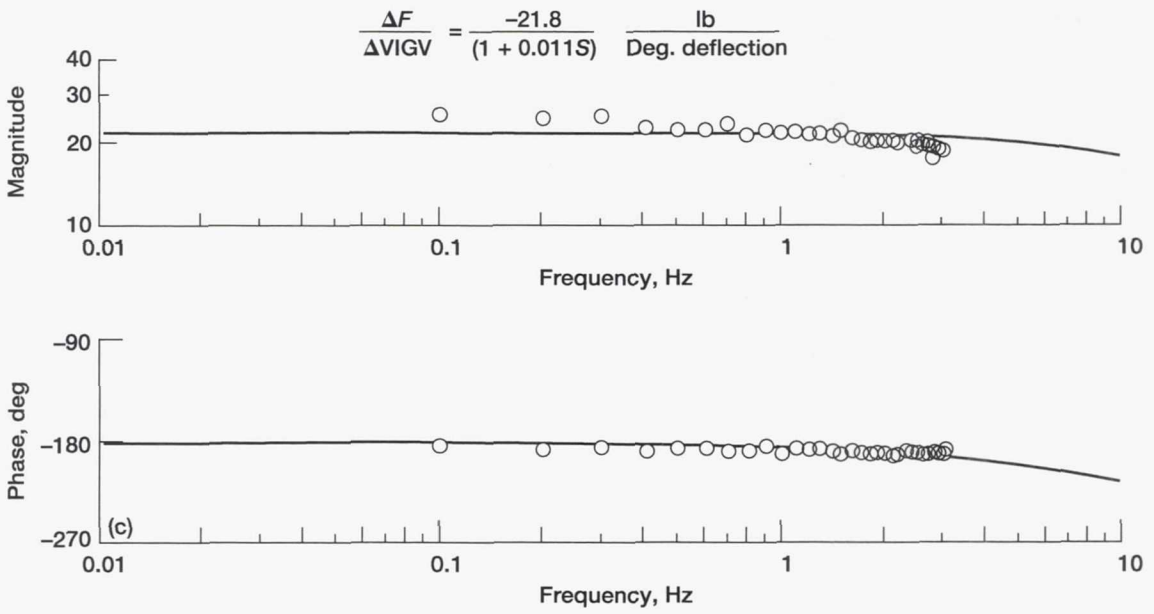

Figure 21.—Concluded. (c) Thrust response.

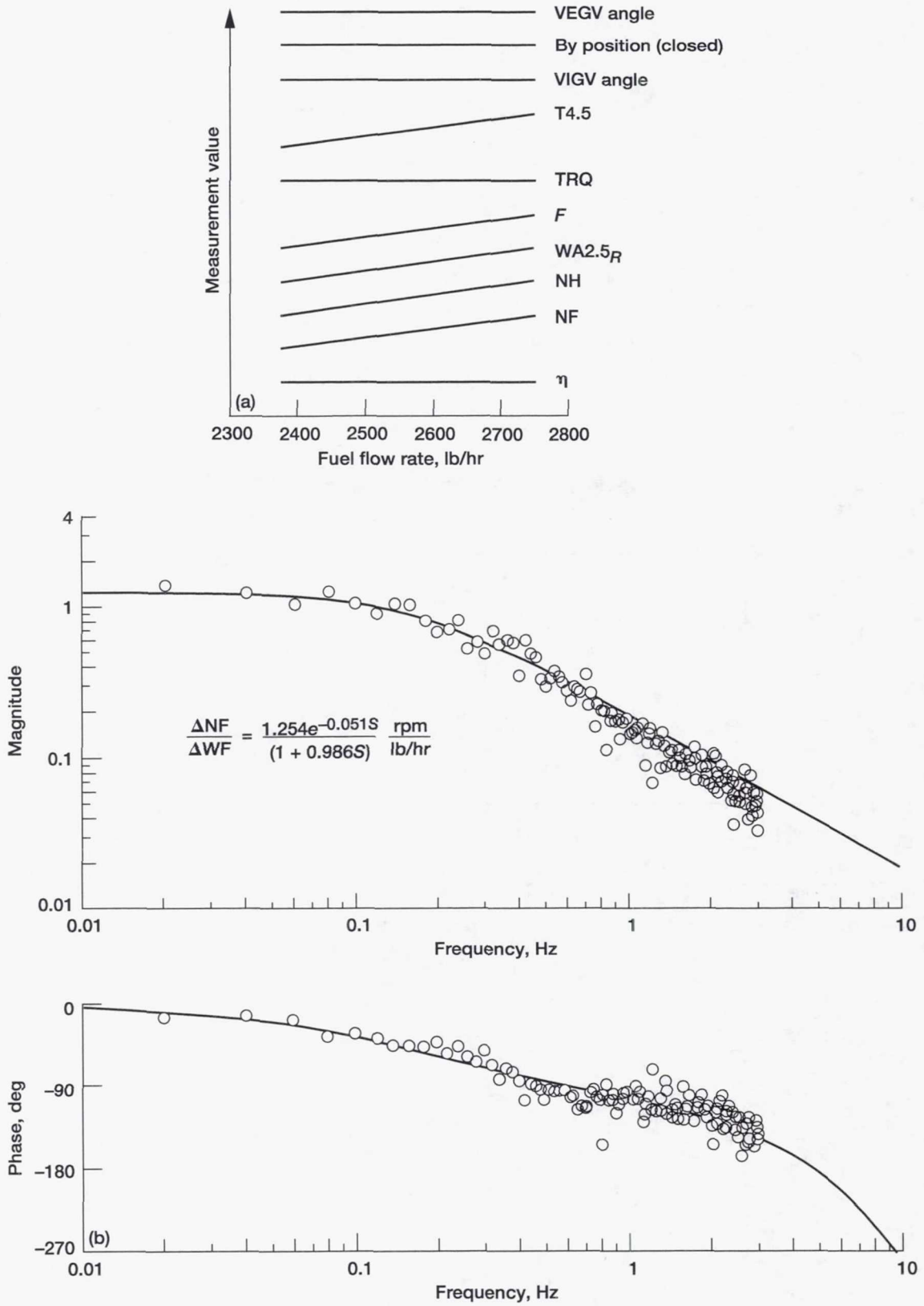

Figure 22.—Open-loop tests with small VIGV perturbations in shaft mode: VIGV open (0°); T4.5 ≃$T4.5_{max}$; NF ≃ 90 percent; PWSD ≃ 400 hp; anticipation circuits and power priority bias off. (a) Steady-state calibration. (b) Fan speed response. (c) Core speed response. (d) T4.5 response. (e) Thrust response.

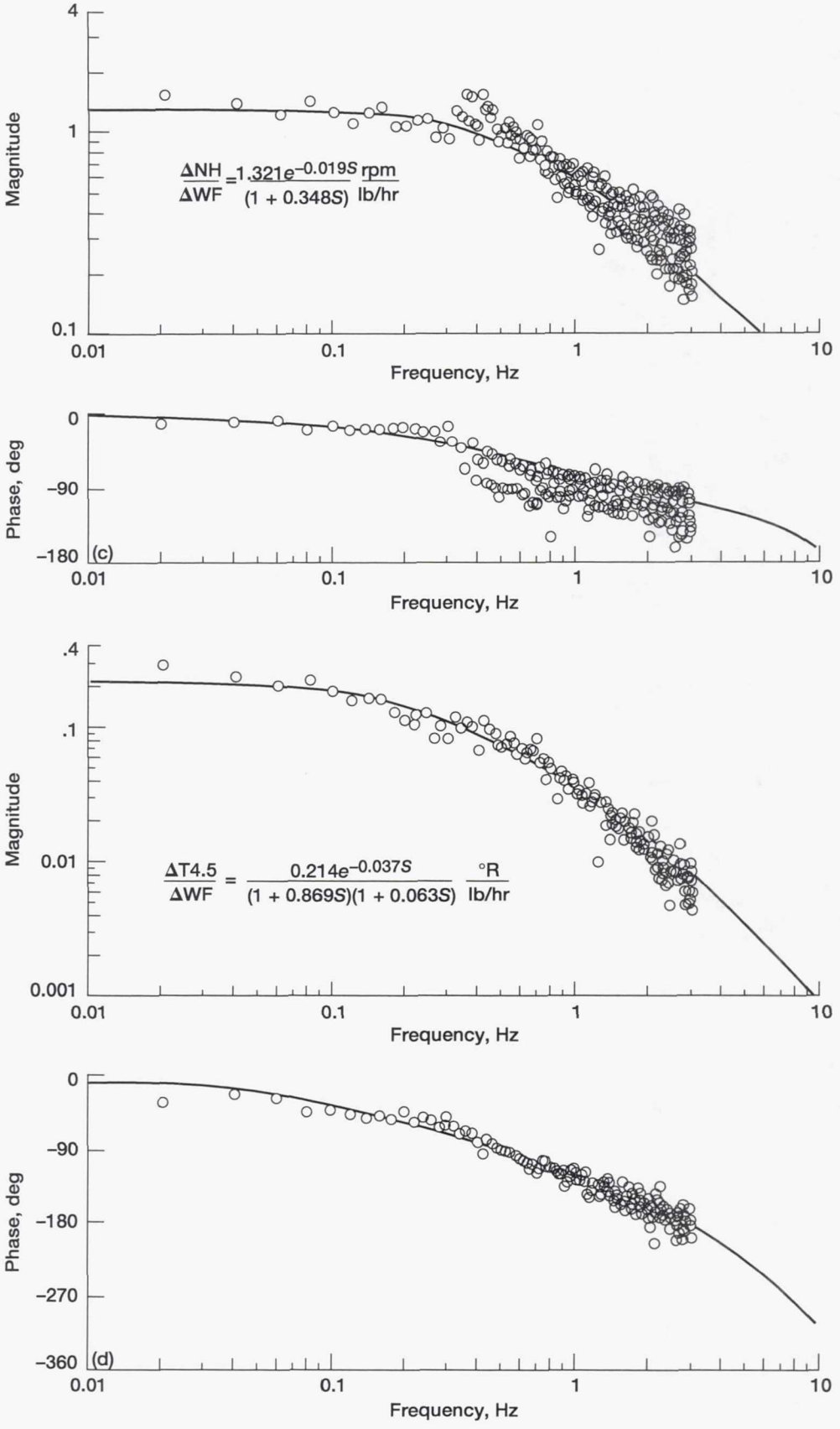

Figure 22.—Continued. (c) Core speed response. (d) T4.5 response.

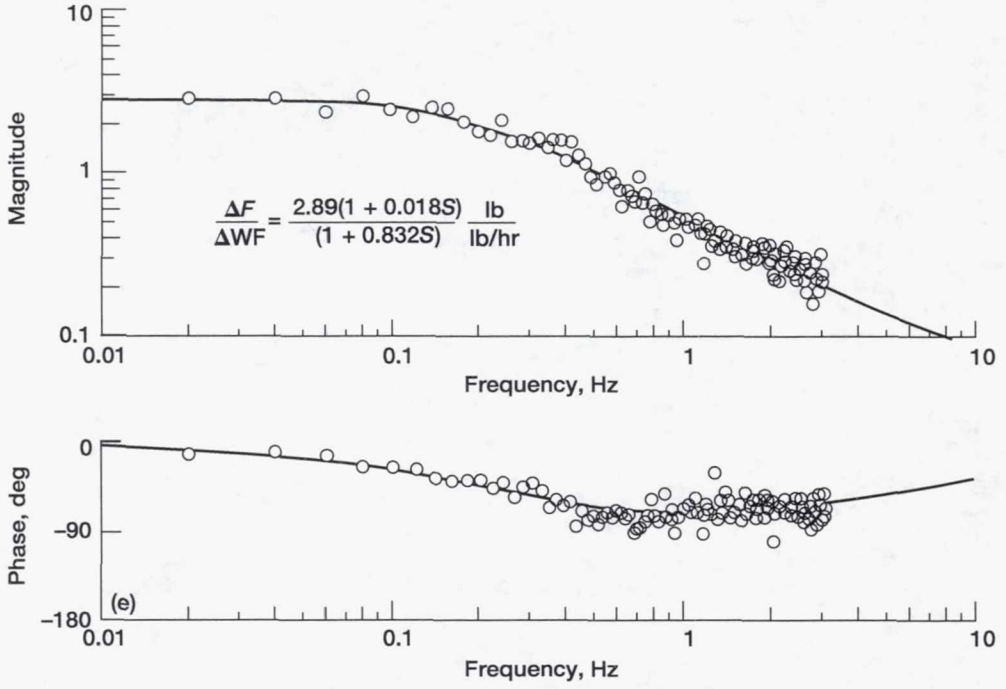

Figure 22.—Concluded. (e) Thrust response.

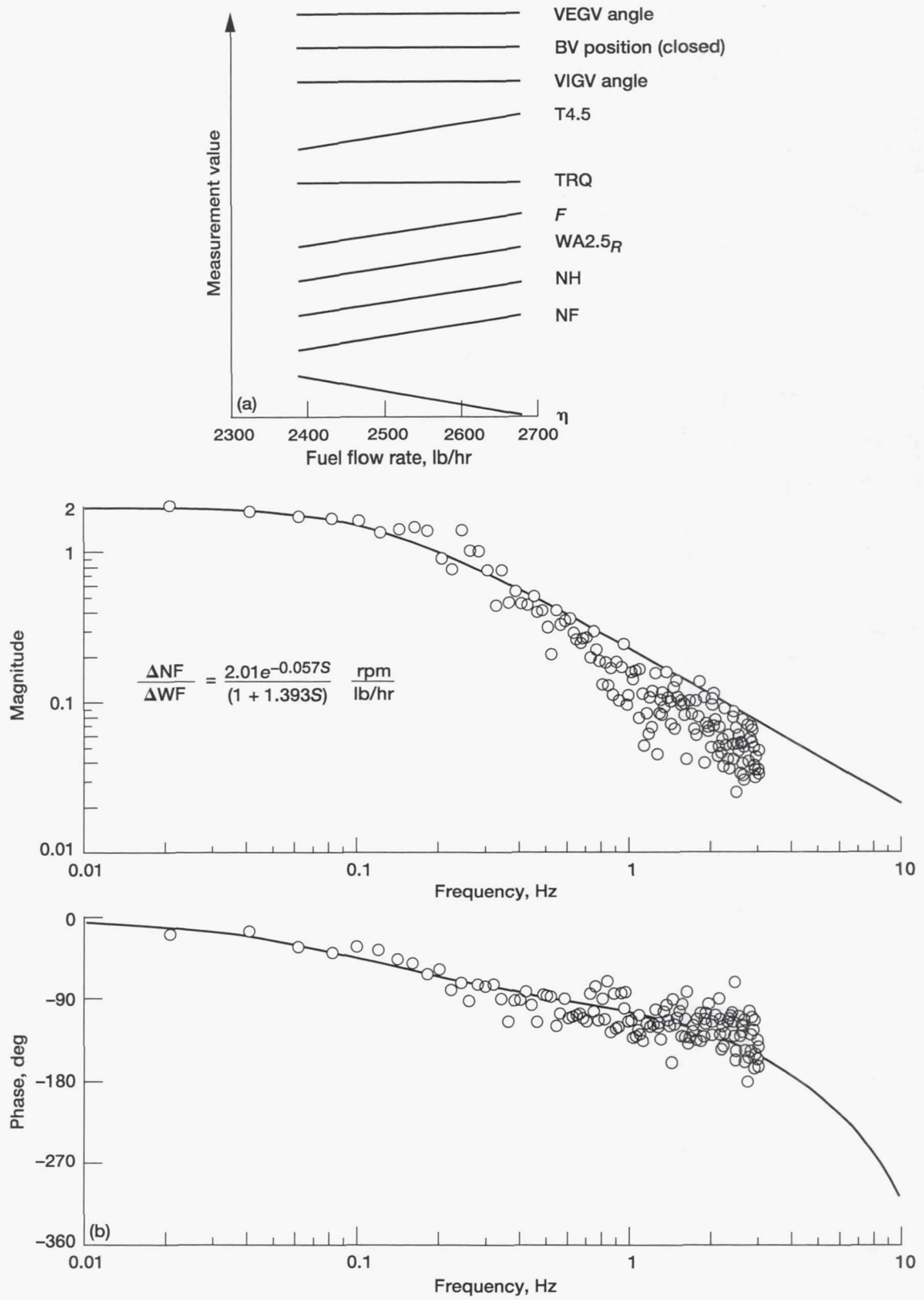

Figure 23.—Open-loop tests with small WF perturbations in shaft mode: VIGV closure, 75 percent (65°); T4.5 ≈$T4.5_{max}$; NF ≈ 90 percent; PWSD ≈ 2800 hp; anticipation circuits and power priority bias off. (a) Steady-state calibration. (b) Fan speed response. (c) Core speed response. (d) T4.5 response. (e) Thrust response.

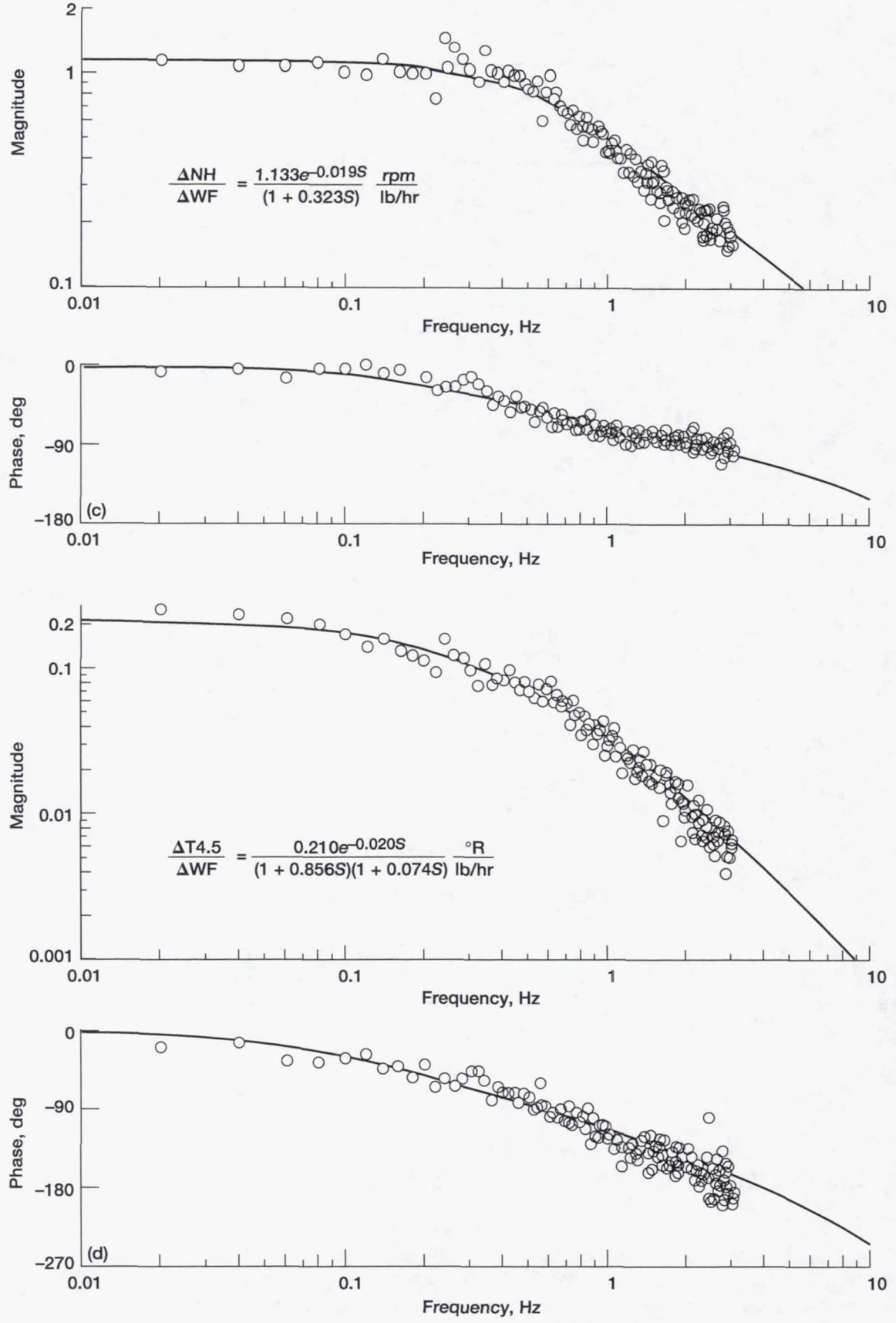

Figure 23.—Continued. (c) Core speed response. (d) T4.5 response.

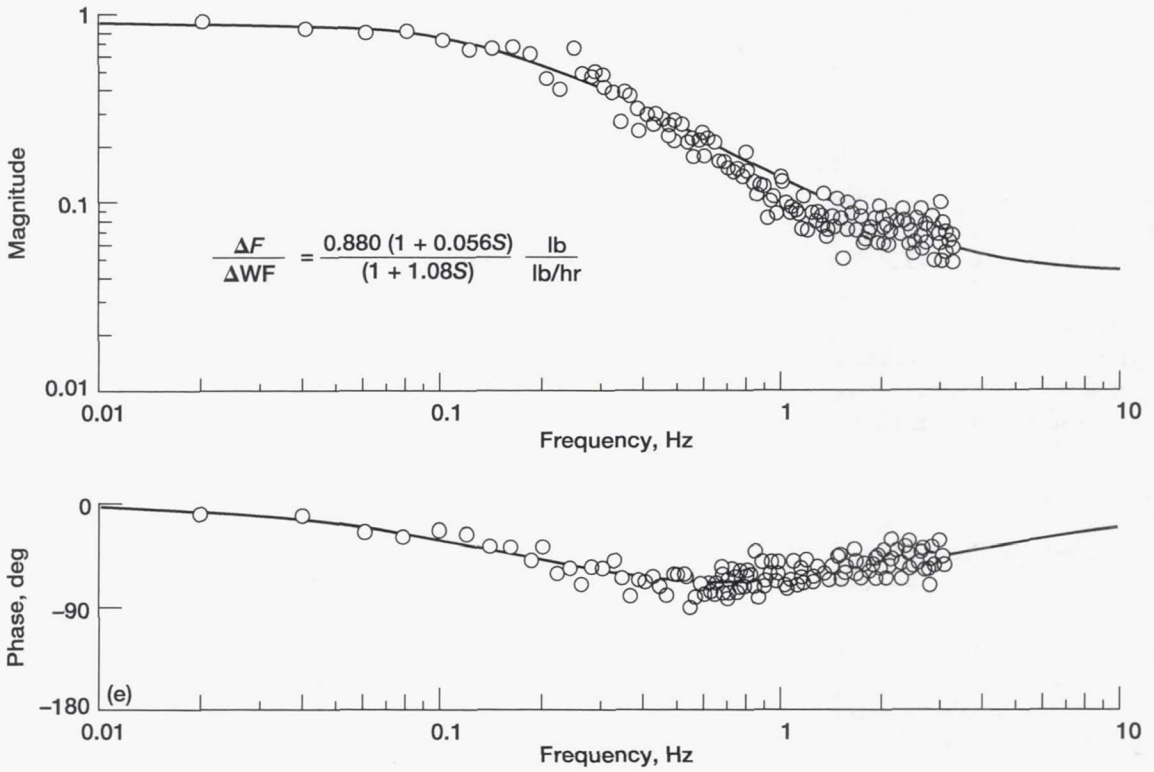

Figure 23.—Concluded. (e) Thrust response.

Data interpretation can be made in a similar manner as detailed in the preceding discussion.

Concluding Remarks

The CEST TF34 convertible engine, equipped with a specially designed digital control system, successfully completed all planned testing on an outdoor static test stand at the NASA Lewis Research Center. Steady-state and acoustic test results have been reported in previous NASA publications. Significant results of transient and dynamic performance tests reported herein are as follows:

1. The engine ran safely and stably through all the tests.

2. Transient tests were performed at 95-percent fan speed to explore engine behavior throughout the operating envelope. The tests included large torque and thrust steps in the shaft control mode, large thrust steps in the thrust control mode, and several combined thrust and torque changes. The steps were up to 4500 lb in thrust and 2500 ft-lb in torque. Features of the digital control system, such as the anticipation circuits and speed control loops, were demonstrated during the tests. A consistent but unexplained 80- to 120-msec dead time between the command signal and the beginning of engine geometry and fuel flow changes was observed during these tests.

3. Open-loop (engine alone) transfer functions were obtained by using the pseudorandom binary noise testing technique. The transfer functions describe engine dynamic behavior for variable inlet guide vane and fuel flow perturbations. The transfer functions can be useful for designing future convertible engines and their associated control systems.

4. A power absorber system using a waterbrake dynamometer was a satisfactory engine power output shaft load for these tests. The system was operated up to 5300 hp. The closed-loop frequency response for torque-demand input was flat to approximately 4 Hz but showed up to 50-msec dead time. No explanation is known to account for the dead time, but the dead time had little effect on these test results.

Lewis Research Center
National Aeronautics and Space Administration
Cleveland, Ohio, June 10, 1995

Appendix A

Power Absorber System Performance

Waterbrake

The waterbrake dynamometer, shown schematically in figure 24, consists of a rotor that spins between stator plates in a housing. The rotor is an assembly of disks mounted on a shaft. Cold water enters the waterbrake around the shaft and is thrown radially outward by the rotor. Holes in the disks and stator plates generate high turbulence. The water forms an annular shape that rotates at about half the rotor speed and then flows out through exit ports in the housing. The rotor drag, which causes torque on the shaft, increases as the depth of the annulus becomes greater. The power absorbed by the waterbrake is the product of torque and rotor speed. Power is converted to heat, which is carried away by the water.

The depth of the water annulus, called the water level, is controlled by valves in the inlet or exit lines. The inlet valve controls the water throughflow and therefore controls the water level and the temperature rise for a given power absorption. The exit valve controls the water level by setting the pressure needed to pump water out of the system. Both valve functions are necessary for waterbrake operation, but torque can be varied by adjusting either valve.

Torque Control With Inlet Water Valve

An initial power absorber system was set up as sketched in figure 25. In this configuration a three-way inlet water valve was used to keep constant water flow in the long line to the cooling tower water source. The intent was to minimize water inertia effects on waterbrake operation. An orifice in the exit line restricted water outlet flow. The steady-state performance of this system is shown in figure 26. For each exit orifice size, both shaft torque and water flow rate increased as the valve was opened. When the waterbrake rotor became "fully wetted" (i.e., the water level extended from the housing all the way to the shaft to completely submerge the rotor disks), the torque limit was reached and the water flow rate became constant. The steady-state performance was nearly independent of shaft speed. With this type of water level control the

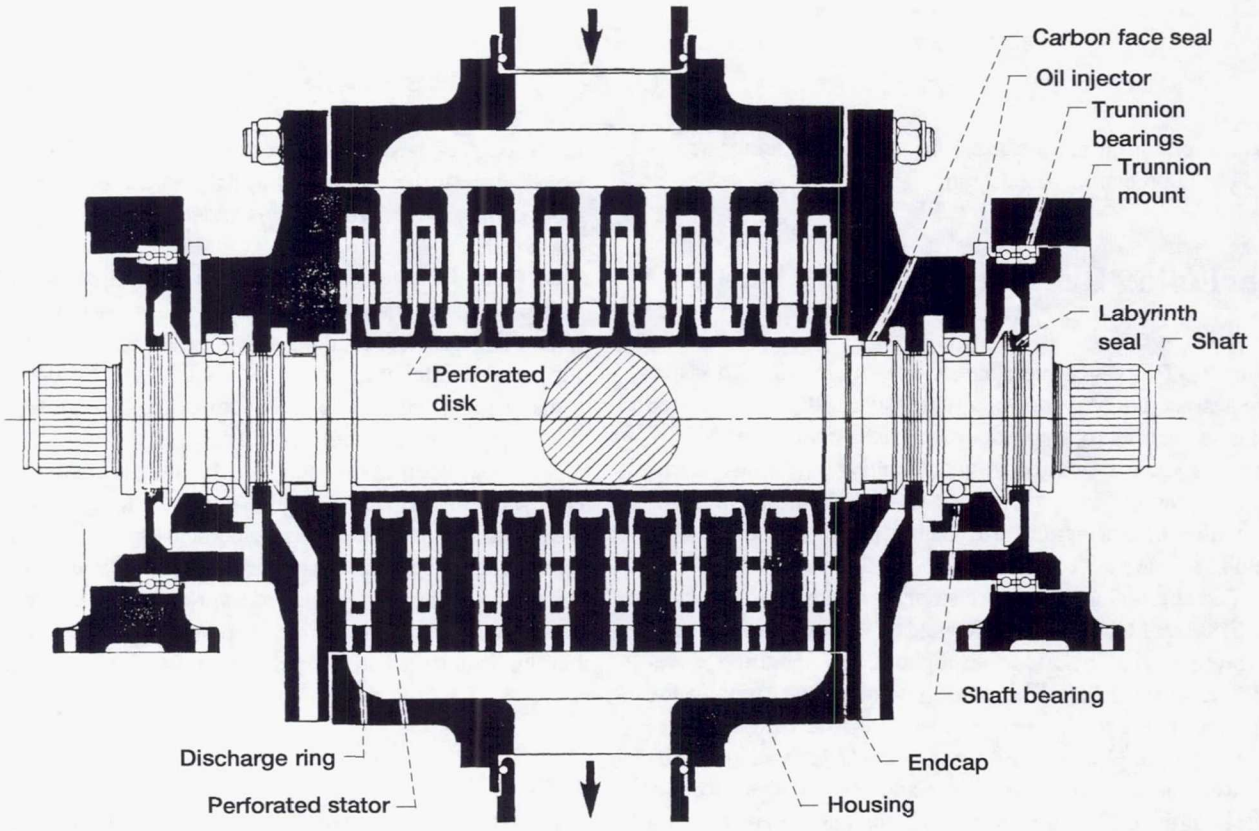

Figure 24.—Schematic of Kahn Industries, Inc., model 108–130 waterbrake dynamometer.

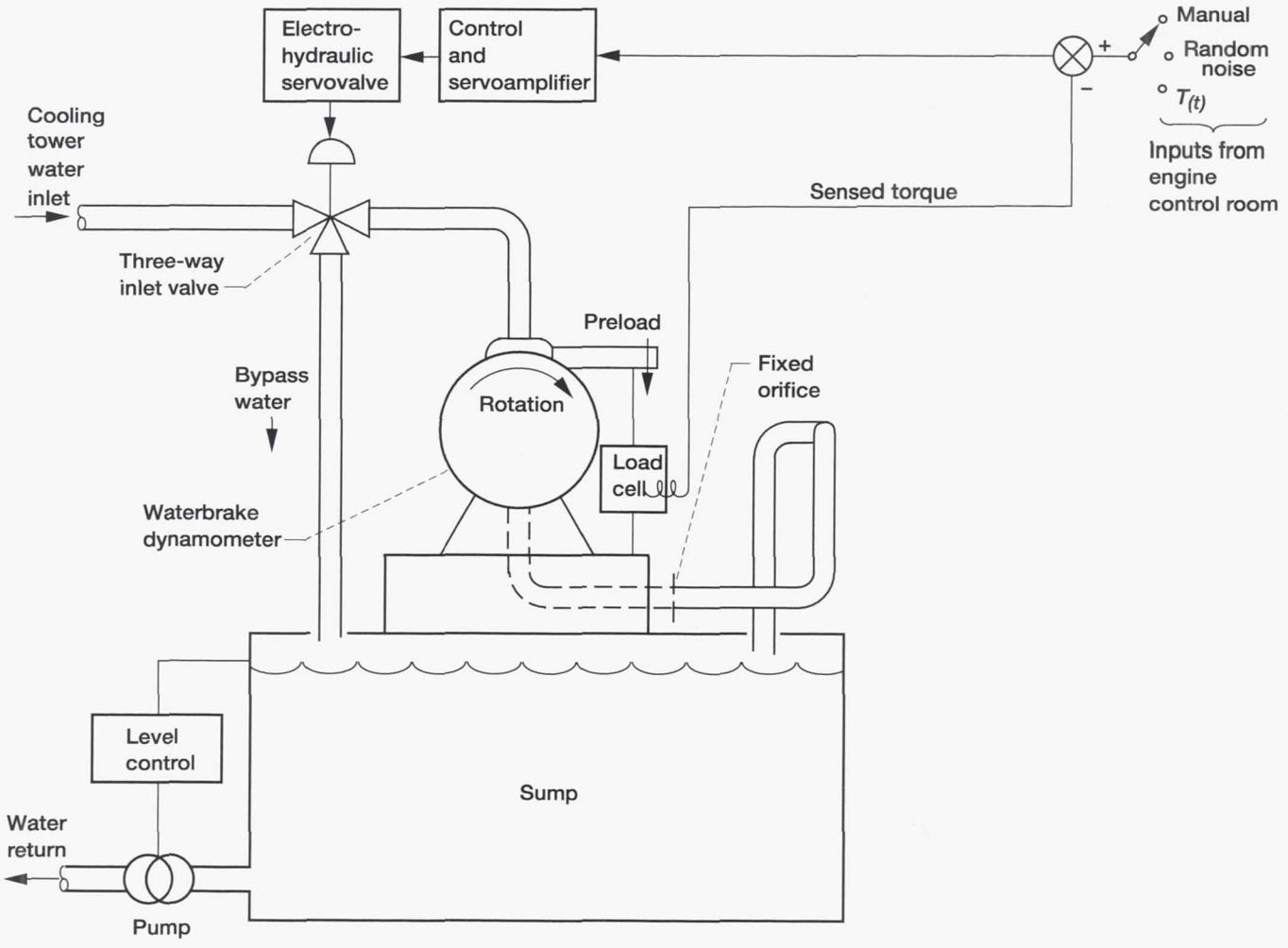

Figure 25.—Waterbrake setup with control valve at inlet. (This setup was not used for engine performance reported herein.)

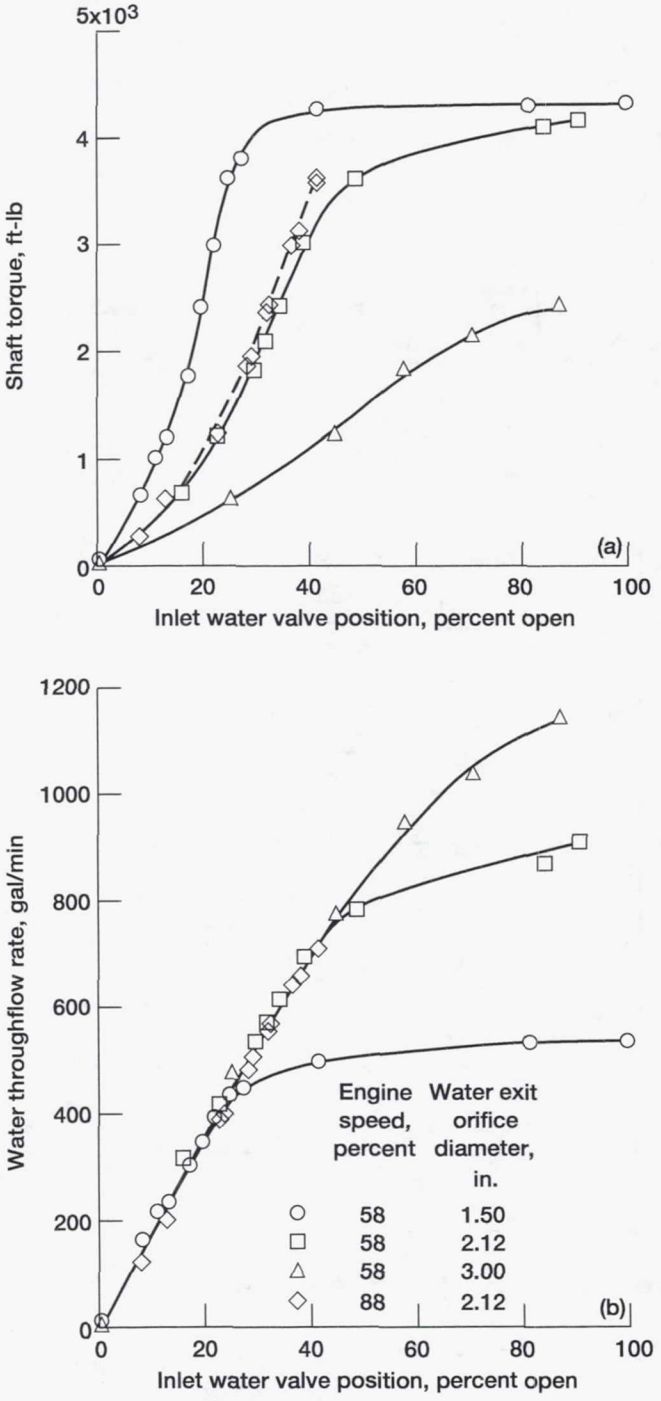

Figure 26.—Waterbrake steady-state performance with control valve at inlet (see fig. 25). (a) Torque. (b) Water flow rate.

orifice size must be chosen to ensure that the rotor does not become fully wetted during dynamic testing.

The three-way inlet water valve was operated by a hydraulic actuator. No small-perturbation frequency response tests of this valve/actuator combination were made; however, from some step-input tests it was estimated that the valve/actuator was critically damped and had approximately 6-Hz natural frequency. The dynamic performance of this system configuration is given in figure 27. Time responses to step inputs (fig. 27(a)) show that after approximately 50-msec dead time the torque changed relatively smoothly to the new level. Initial torque response was faster for a valve-open than for a valve-closed step, indicating that the waterbrake filled more quickly than it emptied. The frequency response transfer function (fig. 27(b)) was deduced from numerical analysis of the step-input response data. The function given includes the inlet water valve dynamics previously described.

Other data obtained with this power absorber configuration consistently showed about 50-msec dead time in torque response. Although no firm explanation could account for this, it was believed to be related to the presence of an air space in the vertical portion of the inlet line between the three-way valve and the waterbrake. Calculations showed that this line, made from large-diameter pipe, did not flow fully. In an effort to improve the waterbrake response by eliminating the dead time, the control valve was moved to the exit side.

Torque Control With Exit Water Valve

The power absorber system using a control valve in a water exit line is sketched in figure 4. This system was used for all the tests described in this report. The valve was installed in a trap in the water line to ensure that it was always submerged. The steady-state performance of this system is shown in figure 28. For each fixed setting of the inlet water valve the water flow rate was constant. As the exit valve was closed, the torque increased in a nonlinear manner and was not affected by engine speed. Note that low torque was obtained only with small inlet valve openings (as exemplified by the circle symbols in fig. 28). Thus, ramp changes in valve position, such as were used for the transient test torque commands, produced very nonlinear demands on the engine when the torque command changes were large.

The two-way valve in the exit water line was 4-in. size with a linear plug. It was moved by a hydraulic actuator moving a 2.5-in. cylinder and with a 2.5-in. stroke. The hydraulic working pressure was 2800 psig. The open-loop frequency response of this valve and actuator, shown in figure 29, was flat to approximately 10 Hz. The dynamic performance of this system configuration is shown in figure 30. This system was faster than the system with the inlet water control valve, as shown by comparing figures 27(a) and 30(a). However, this configuration also exhibited a significant dead time. No satisfactory explanation for the dead time is known. The open-loop frequency response of the combined valve and waterbrake system from PRBN tests is shown in figure 30(b). The valve response (fig. 29) was much faster than this combined response; thus, the frequency response shown in figure 30(b) closely approximated the response of the waterbrake alone.

A system performance comparison from these test results is as follows:

	Inlet water valve	Exit water valve
Water valve		
Natural frequency, Hz	6	13.8
Damping factor	1	0.62
Waterbrake		
Time constant, sec	0.43	0.145
Dead time, sec	0.050	0.024

For the valves used, the waterbrake dynamics dominated performance. The results indicate that performance was better with the control valve in the exit line. However, the dead time measured in these tests precluded simulation of dynamic inertia shaft loads using derivative torque feedback because the waterbrake was unstable when operated with the engine control system. The waterbrake dead time may also limit its use for other types of transient or dynamic testing.

Closed-Loop Torque Response

Using the power absorber configuration with the control valve in the water exit line (fig. 4), the control loop was closed with proportional-plus-integral electronics and adjusted for best performance. The time response (fig. 31(a)) was better than 12 000 ft-lb/sec. Dead time was still present. The frequency response (fig. 31(b)) was flat to more than 3 Hz, reflecting the improved bandwidth expected from the properly adjusted closed-loop control.

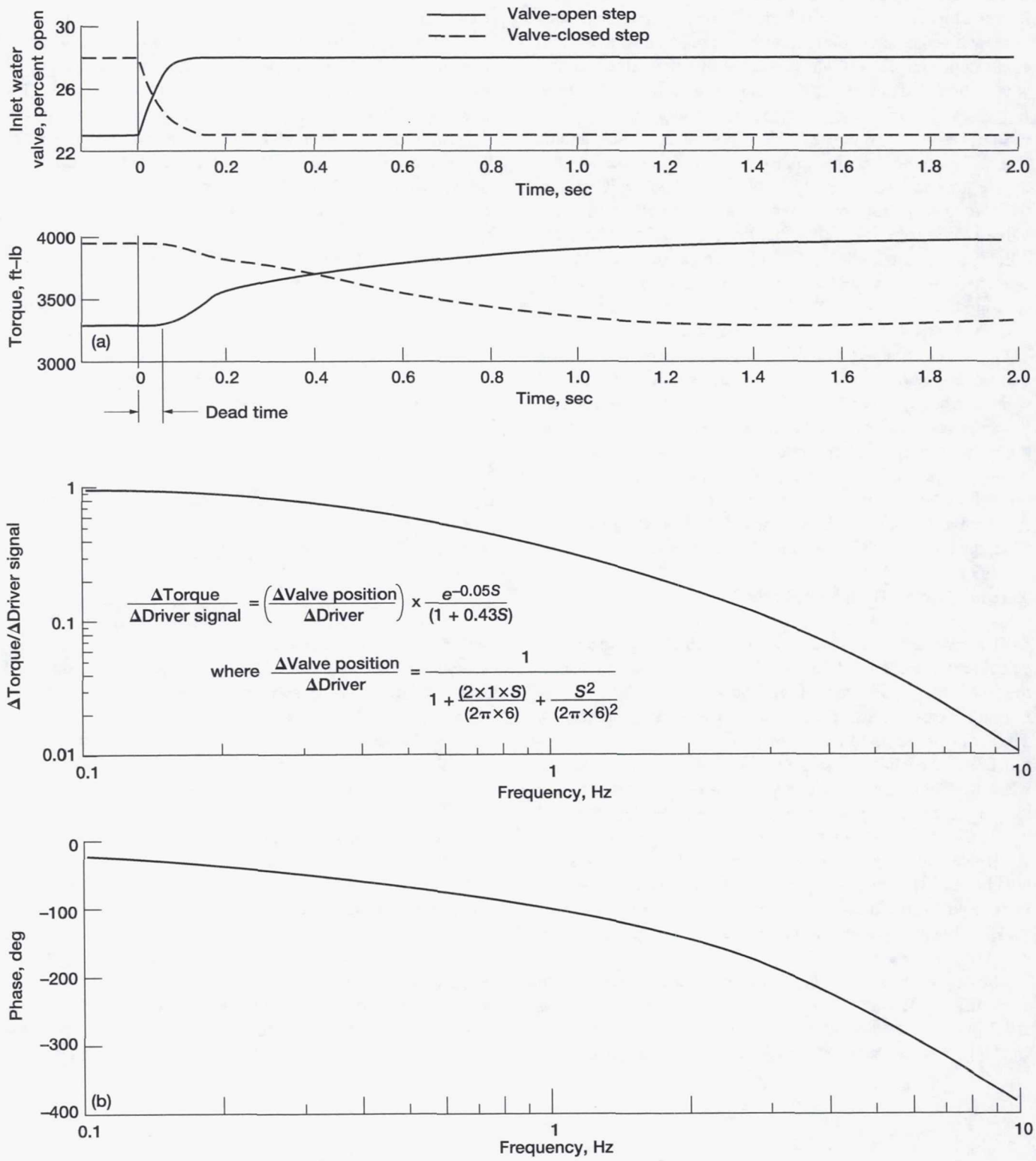

Figure 27.—Waterbrake dynamic performance with control valve at inlet. (a) Time responses. For each case, driver was a step input to valve at inlet. (b) Open-loop torque frequency response from numerical analysis of step-input response.

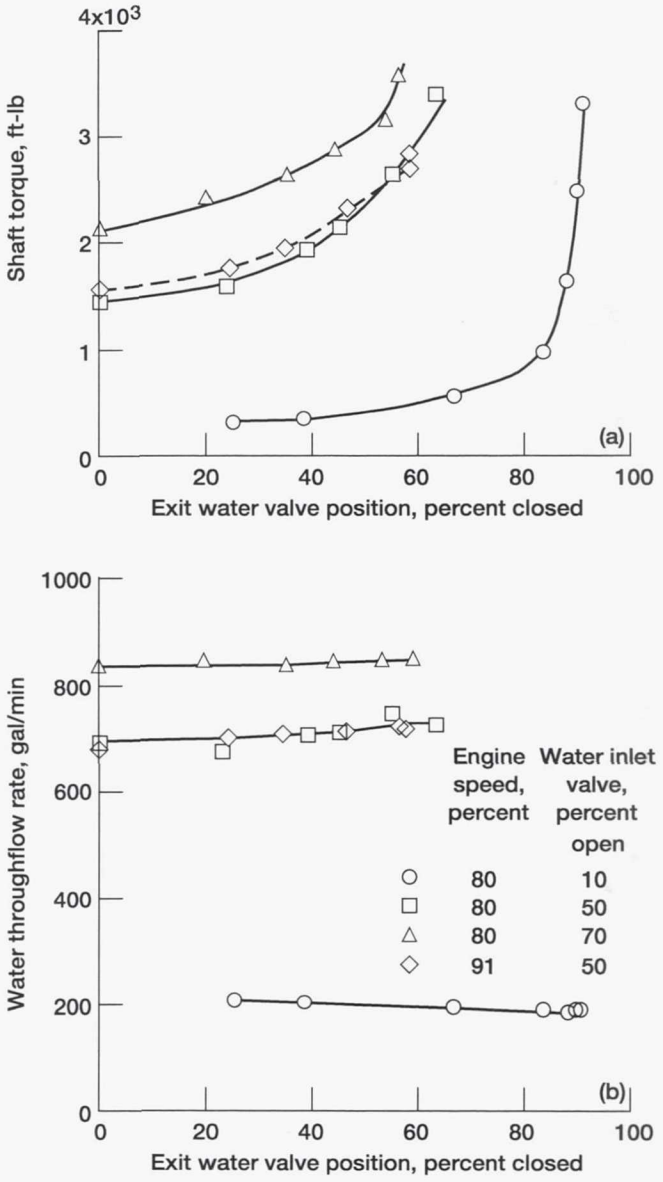

Figure 28.—Waterbrake steady-state performance with control valve at exit (see fig. 4). (a) Torque. (b) Water flow rate.

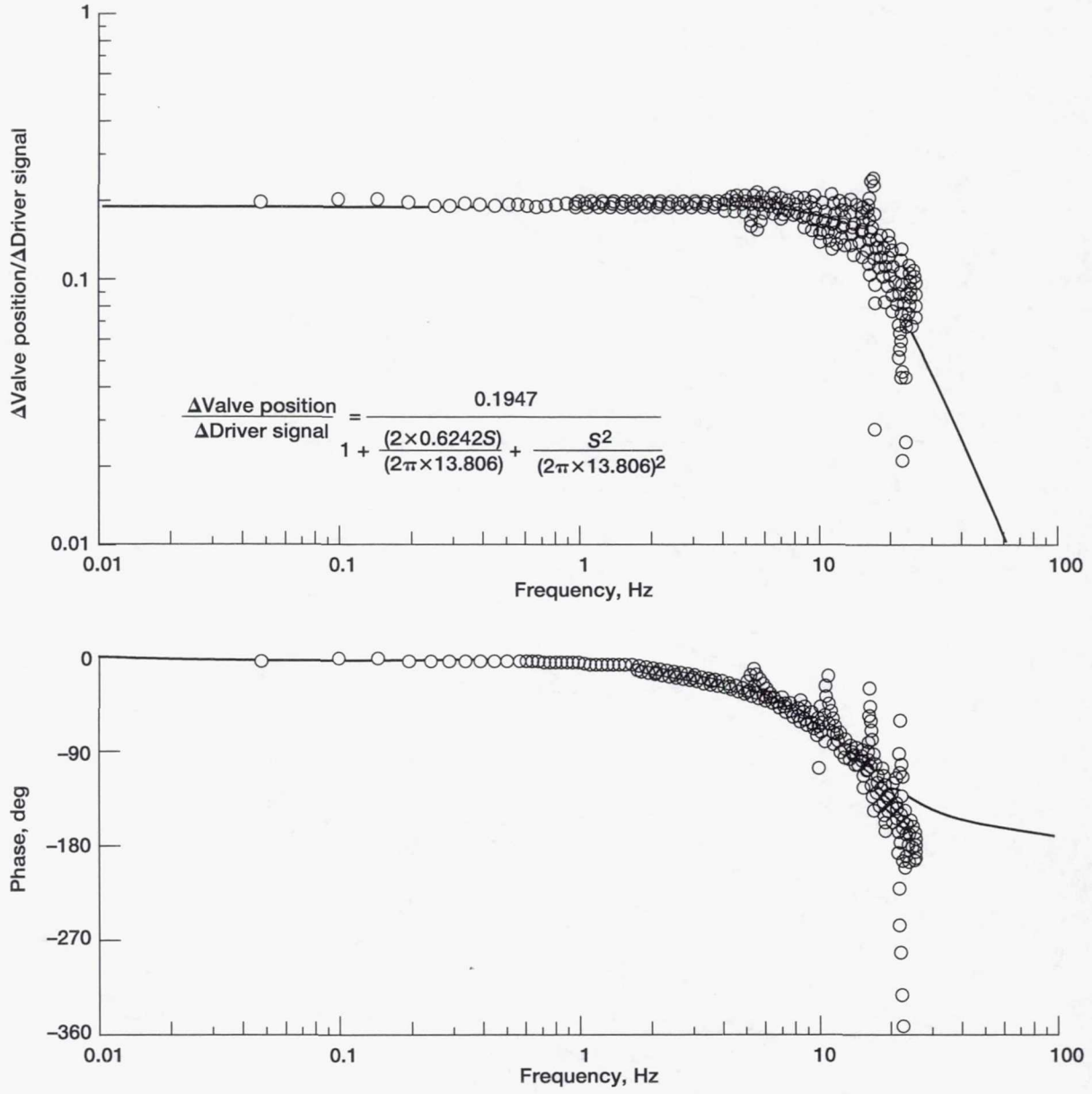

Figure 29.—Open-loop torque frequency response of control valve (two-way) at exit.

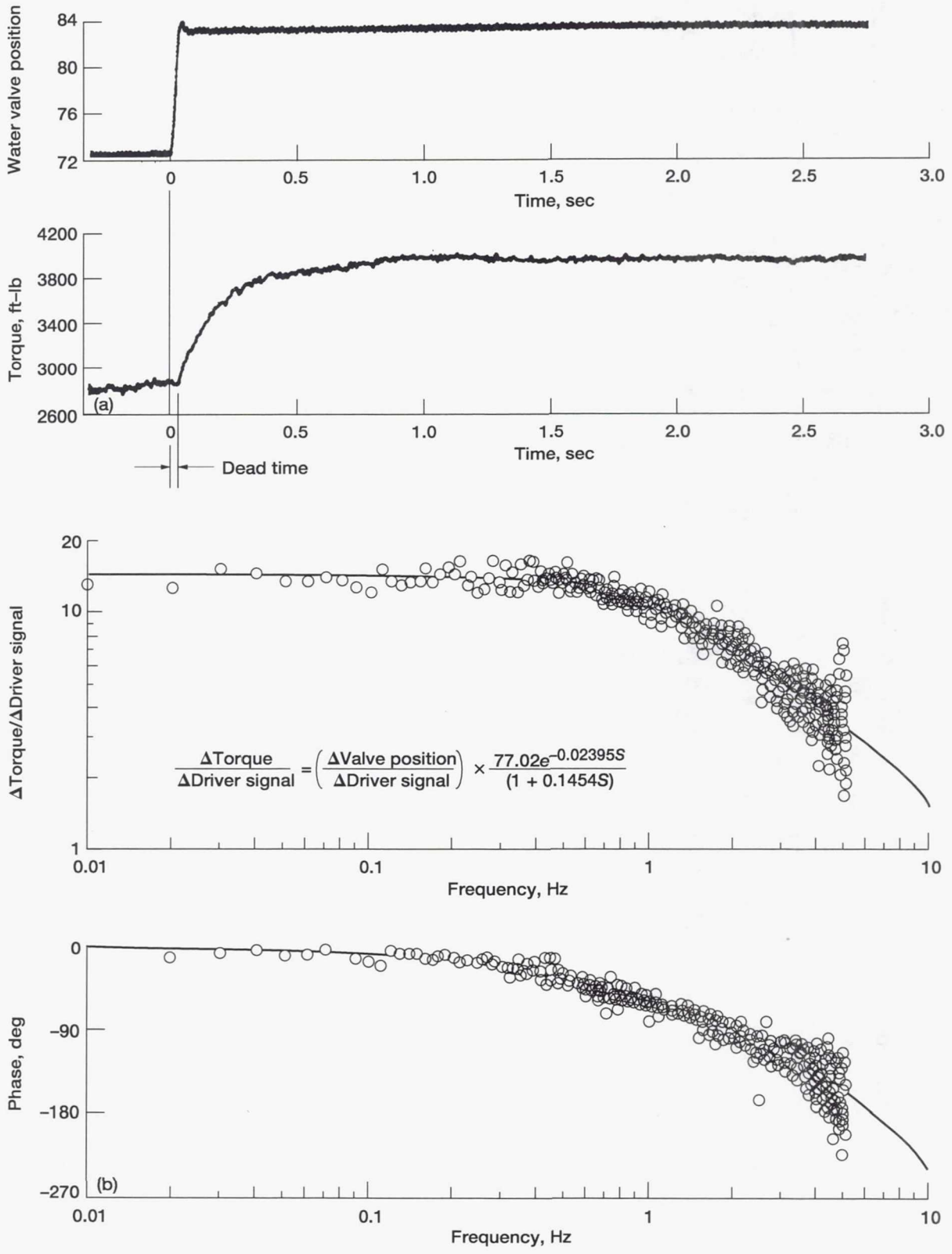

Figure 30.—Waterbrake dynamic performance with control valve at exit. (a) Time response. (Driver was a step input to valve at time = 0 sec.) (b) Open-loop frequency response from PRBN input to valve.

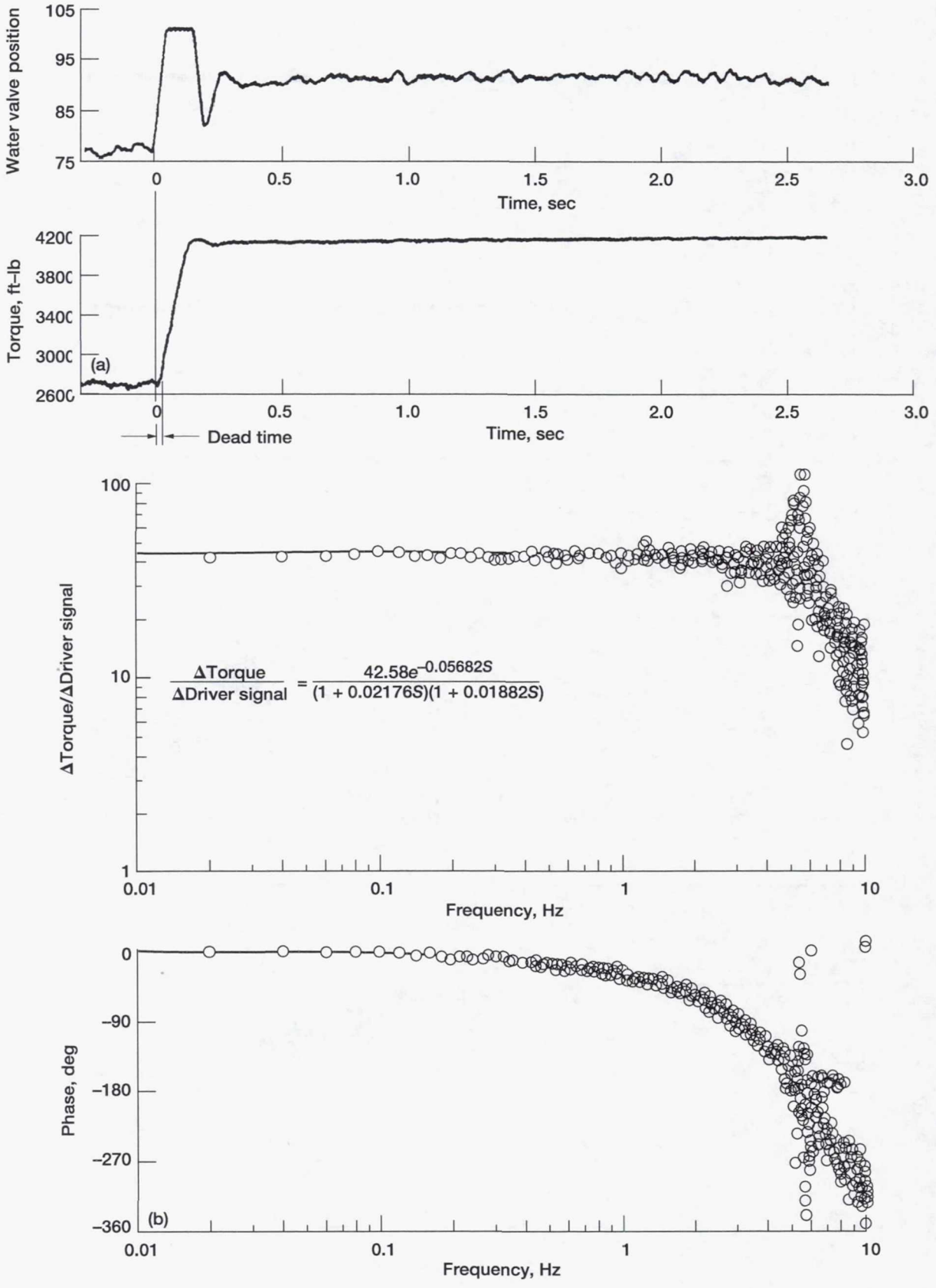

Figure 31.—Closed-loop response of power absorber system with control valve at waterbrake exit. Proportional-plus-integral control. (a) Time response. (Driver was a step input to valve at time = 0 sec.) (b) Frequency response.

Appendix B

Pseudorandom Binary Noise Generator

The pseudorandom binary noise (PRBN) method was chosen for the small-perturbation frequency response tests. The PRBN method is quicker than the sine-sweep method, and previous test experience has shown that results from the two methods compare satisfactorily (refs. 16 and 17).

The PRBN generator block diagram is shown in figure 32(a). An electronic bit generator, using a 10-bit shift register running at a preset clock frequency, produced pulses of random width and spacing. The pulse changes occurred at clock intervals. The pulses drove a dynamic system that perturbed the plant. Use of the PRBN generator to perturb the VIGV system is illustrated in figures 32(b) to (d). The bit generator signal consisted of random sharp-edge pulses. The vane motion resulting from this signal was slightly rounded because of the relatively high clock frequency. The frequency spectrum of the vane position indicates the random changes detected by the engine. The first cusp-shaped minimum occurred at the clock frequency, 5.5 Hz, as expected by theory (ref. 17). Also, from theory, the minimum frequency present in the perturbation was

$$\frac{\text{Clock frequency}}{2^{10}-1} = 0.005 \text{ Hz}$$

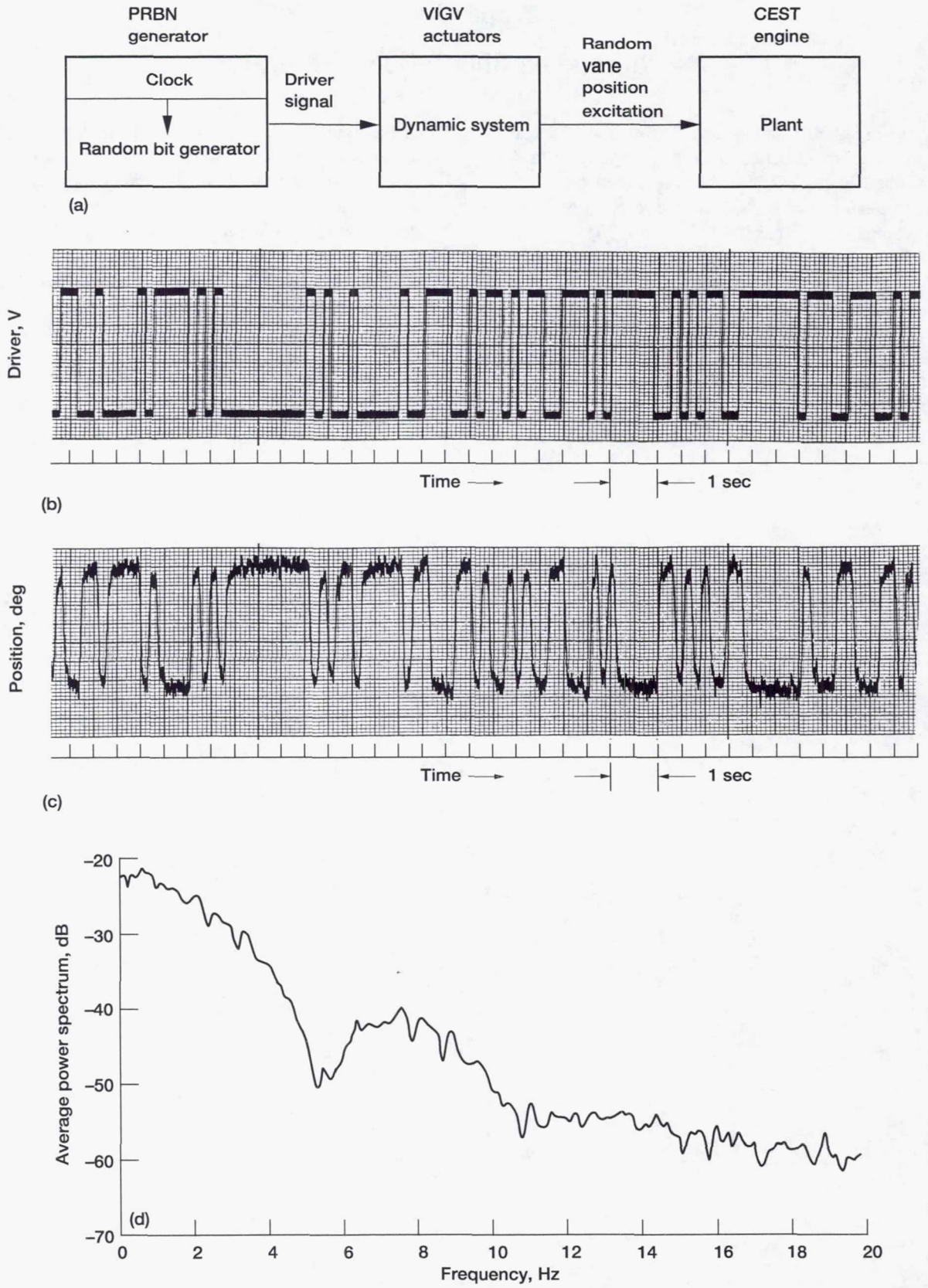

Figure 32.—VIGV driven by PRBN generator for frequency response tests. (a) Block diagram. (b) Driver signal. (c) Vane position. (d) Power spectrum of vane position.

Appendix C

Symbols

F	engine gross thrust,[1] lb
F_R	referred engine gross thrust,[1] F/δ
NF	fan, power-output-shaft, and power-turbine speed, percent of 6890 rpm
NF_{max}	maximum fan operating speed, rpm
NF_R	referred fan, power-output-shaft, and power-turbine speed, NF/$\sqrt{\theta}$, percent of 6890 rpm
NH	core-engine speed, rpm
PS3	core compressor discharge pressure, psia
PWSD	output shaft power, hp
$PWSD_R$	referred output shaft power, PWSD/$\delta\sqrt{\theta}$
S	LaPlacian operator
T	temperature, °R
TRQ	output shaft torque, ft-lb
$T_{(t)}$	torque control system input signal from programmable signal generator
T4.5	power-turbine inlet total temperature, °R
$T4.5_{max}$	limiting power turbine inlet temperature, °R
WA2.5	core airflow, lb/sec
$WA2.5_R$	referred core airflow, WA2.5 $\sqrt{\theta}/\delta$
WF	fuel flow rate, lb/hr
WF_R	referred fuel flow rate, WF/$\delta\theta$
δ	ratio of pressure to 14.696 psi
θ	ratio of temperature to 518.7 °R
η	fan tip adiabatic compression efficiency

[1]Called "gross thrust" because, by convention with the TF34 engine, the reported thrust is net (measured in test stand) thrust plus calculated core cowling scrubbing drag.

References

1. Eisenberg, J.D.: Rotorcraft Convertible Engines for the 1980's. NASA TM–83008, 1982.
2. Goldstein, D.N.; Hirschkron, R.; and Smith, C.E.: Rotorcraft Convertible Engine Study. (R83AEB047, General Electric Co.; NASA Contract NAS3–22743.) NASA CR–168241, 1983.
3. Abdalla, K.L.; and Brooks, A.: TF34 Convertible Engine System Technology Program. Proceeding of the 38th Annual Forum, American Helicopter Society, 1982, pp. 163–169.
4. Quiet Clean Short-Haul Experimental Engine (QCSEE) Under-the-Wing (UTW) Engine Composite Nacelle Test Report. (R78AEG573–Vol. 1, General Electric Co.; NASA Contract NAS3–18021.) NASA CR–159471, 1979.
5. Schaefer, J.W.; Sagerser, D.R.; and Stakolich, E.G.: Dynamics of High-Bypass-Engine Thrust Reversal Using a Variable-Pitch Fan. NASA TM X–3524, 1977.
6. Jones, B.A.; and Wright, D.L.: Convertible Fan/Shaft Engine Variable Fan Geometry Investigation. USAAVLABS–TR–70–28, PWA–FR–3567, Pratt & Whitney Aircraft, 1970.
7. Bobula, G.A.; Soeder, R.H.; and Burkardt, L.A.: Effect of a Part-Span Variable Inlet Guide Vane on the Performance of a High-Bypass Turbofan Engine. AIAA Paper 81–1362, July 1981.
8. Williams, R.M.; and Boyd, T.H.; Preliminary X-Wing Characteristics and Interface Document. DTNSRDC/TM–16–81/06, David W. Taylor Naval Ship Research and Development Center, May 1981.
9. Biggers, J.C.; and Linden, A.W.: X-Wing—A Low-Disc-Loading V/STOL for the Navy. SAE Paper 851772, Oct. 1985.
10. Gill, J.C.; Earle, R.V.; and Mar, H.M.: Rotorcraft Convertible Engine Study. (DDA–EDR–10978, Detroit Diesel Allison; NASA Contract NAS3–22742.) NASA CR–168161, 1982.
11. Eisenberg, J.D.; and Bowles, J.V.: Folding Tilt Rotor Demonstrator Feasibility Study. Proceedings of the 42nd Annual Forum, American Helicopter Society, Vol. 2, 1986.
12. McArdle, J.G.; Barth, R.L.; and Burkardt, L.A.: Steady-State Performance of a Turbofan/Turboshaft Convertible Engine With Variable Inlet Guide Vanes. NASA TP–1673, 1987.
13. McArdle, J.G.: Fan Acoustic Characteristics of a Turbofan/Turboshaft Convertible Engine With Variable Inlet Guide Vanes. NASA TM–100207, 1987.
14. Gilmore, D.R., Jr.: TF34 Convertible Engine Control System Design. Proceedings of the 40th Annual Forum, American Helicopter Society, 1984, pp. 609–620.
15. Seidel, R.C.: Transfer-Function-Parameter Estimation From Frequency Response Data—A FORTRAN Program. NASA TM X–3286, 1975.
16. de los Reyes, G.; and Gouchoe, D.R.: The Design of a Turboshaft Speed Governor Using Modern Control Techniques. (General Electric Co.; NASA Contract NAS3–22763.) NASA CR–175046, 1986.
17. Cottington, R.V.; and Pease, C.B.: Dynamic Response Testing of Gas Turbines. J. Eng. Power, Jan. 1979.

REPORT DOCUMENTATION PAGE

Form Approved
OMB No. 0704-0188

1. AGENCY USE ONLY (*Leave blank*)	2. REPORT DATE	3. REPORT TYPE AND DATES COVERED
	April 1996	Technical Memorandum

4. TITLE AND SUBTITLE

Dynamic and Transient Performance of Turbofan/Turboshaft Convertible Engine With Variable Inlet Guide Vanes

5. FUNDING NUMBERS

WU–505–68–30

6. AUTHOR(S)

Jack G. McArdle, Richard L. Barth, Leon M. Wenzel, and Thomas J. Biesiadny

7. PERFORMING ORGANIZATION NAME(S) AND ADDRESS(ES)

National Aeronautics and Space Administration
Lewis Research Center
Cleveland, Ohio 44135–3191

8. PERFORMING ORGANIZATION REPORT NUMBER

E–9637

9. SPONSORING/MONITORING AGENCY NAME(S) AND ADDRESS(ES)

National Aeronautics and Space Administration
Washington, D.C. 20546–0001

10. SPONSORING/MONITORING AGENCY REPORT NUMBER

NASA TM–4696

11. SUPPLEMENTARY NOTES

Responsible person, Thomas J. Biesiadny, organization code 2780, (216) 433–3967.

12a. DISTRIBUTION/AVAILABILITY STATEMENT

Unclassified - Unlimited
Subject Category 07

This publication is available from the NASA Center for Aerospace Information, (301) 621–0390.

12b. DISTRIBUTION CODE

13. ABSTRACT ***(Maximum 200 words)***

A convertible engine called the CEST TF34, using the variable inlet guide vane method of power change, was tested on an outdoor stand at the NASA Lewis Research Center with a waterbrake dynamometer for the shaft load. A new digital electronic system, in conjunction with a modified standard TF34 hydromechanical fuel control, kept engine operation stable and safely within limits. All planned testing was completed successfully. Steady-state performance and acoustic characteristics were reported previously and are referenced. This report presents results of transient and dynamic tests. The transient tests measured engine response to several rapid changes in thrust and torque commands at constant fan (shaft) speed. Limited results from dynamic tests using the pseudorandom binary noise technique are also presented. Performance of the waterbrake dynamometer is discussed in an appendix.

14. SUBJECT TERMS

V/STOL; Controls; Turbofan engines; Turboshaft engines; Propulsion; Convertible engines; Variable inlet guide vanes; VIGV; Waterbrake

15. NUMBER OF PAGES

47

16. PRICE CODE

A03

17. SECURITY CLASSIFICATION OF REPORT	18. SECURITY CLASSIFICATION OF THIS PAGE	19. SECURITY CLASSIFICATION OF ABSTRACT	20. LIMITATION OF ABSTRACT
Unclassified	Unclassified	Unclassified	